AudioCast: Enabling Ubiquitous Connectivity for Embedded Systems through Audio-broadcasting Low-power Tags

RAJASHEKAR REDDY CHINTHALAPANI*, National University of Singapore, Singapore
DHAIRYA JIGAR SHAH*, National University of Singapore, Singapore
NOBEL ANG, National University of Singapore, Singapore
AMBUJ VARSHNEY, National University of Singapore, Singapore

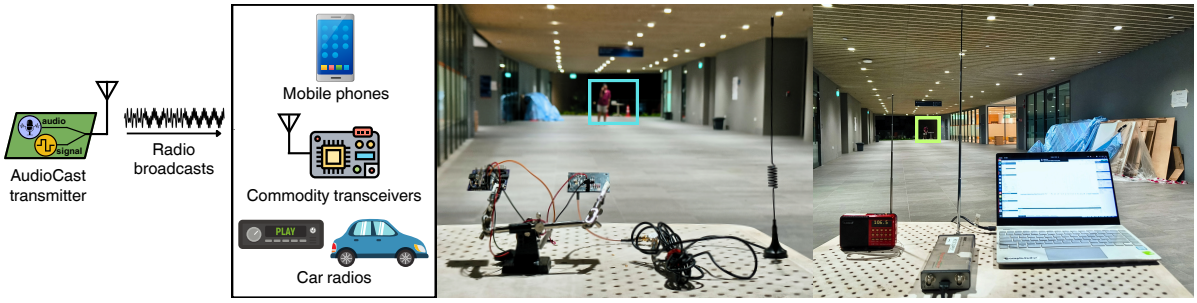

Fig. 1. AudioCast transmitters operate in the FM-broadcast spectrum and transmit information as audio broadcasts. They support a transmission range of up to 130 m in line-of-sight environments and tens of meters in non-line-of-sight environments, while consuming less than 200 µW of power. AudioCast transmissions are compatible with commodity FM-radio receivers, such as those found in cars and smartphones, enabling seamless communication with existing infrastructure.

Wireless connectivity challenges hinder the deployment of embedded systems. We introduce AudioCast to address two critical issues: *spectrum scarcity-induced contention* and *high power consumption in transmitters*. The widespread availability of broadcast radio receivers (for example, FM radios using the 88–108 MHz spectrum) and access to underutilized lower-frequency spectrum motivate the design of AudioCast. The lower-frequency spectrum offers superior radio-wave propagation characteristics, exhibiting at least 10 × lower path loss than the 2.4 GHz and 5 GHz Industrial, Scientific, and Medical (ISM) bands while avoiding congestion and interference. These properties enable reliable and long-distance communication, even for weakly radiated signals. AudioCast builds on these properties and the unique negative resistance of a tunnel diode.

AudioCast rethinks the architecture of radio transmitters using a tunnel diode oscillator to *generate* carrier signals and *self-modulate* them with baseband signals. This results in frequency-modulated transmissions at an overall power consumption below 200 µW. Unlike related systems based on the backscatter mechanism, AudioCast does not require an externally generated carrier or rely on ambient signals. We argue that AudioCast represents an example of a new class of transmitters which we conceptualize as **Beyond-Backscatter** transmitters. Through experiments, we demonstrate that AudioCast achieves a transmission range of up to 130 m in line-of-sight and tens of meters in non-line-of-sight conditions

*Co-primary authors with equal contributions to this work.

Authors' Contact Information: Rajashekar Reddy Chinthalapani, rajashekar.c@u.nus.edu, National University of Singapore, Singapore; Dhairya Jigar Shah, dhairya@u.nus.edu, National University of Singapore, Singapore; Nobel Ang, nobelang78@gmail.com, National University of Singapore, Singapore; Ambuj Varshney, ambujv@nus.edu.sg, National University of Singapore, Singapore.

ACM 2474-9567/2025/6-ART27
https://doi.org/10.1145/3729471

respectively. These transmissions are decodable by ubiquitous commodity FM receivers in cars, homes, and phones. We evaluate AudioCast through theoretical analysis, benchtop experiments, and urban/indoor field deployments. Additionally, we prototype and demonstrate novel applications, including low-power voice transmissions and hand gesture communication, enabled by AudioCast's range and power efficiency.

CCS Concepts: • **Hardware** → **Sensor devices and platforms**; **Wireless devices**; *Networking hardware*; *Sound-based input / output*; • **Computer systems organization** → **Sensor networks**.

Additional Key Words and Phrases: Beyond-backscatter transmitters, FM-broadcast spectrum, Embedded systems

ACM Reference Format:
Rajashekar Reddy Chinthalapani, Dhairya Jigar Shah, Nobel Ang, and Ambuj Varshney. 2025. AudioCast: Enabling Ubiquitous Connectivity for Embedded Systems through Audio-broadcasting Low-power Tags. *Proc. ACM Interact. Mob. Wearable Ubiquitous Technol.* 9, 2, Article 27 (June 2025), 32 pages. https://doi.org/10.1145/3729471

1 Introduction

Embedded systems are ubiquitous: from sensors that monitor our environment [53, 61] to cameras that track our surroundings [51, 52]. As these systems are increasingly being deployed on a scale, their long-term sustainability has become a growing concern [20]. Recent efforts toward sustainable embedded deployments have focused on addressing the power-intensive nature of wireless communication, with the aim of extending battery life [79] or enabling battery-free operation through energy harvesting from ambient sources [15, 30, 76]. These approaches generally reduce power consumption by designing energy-efficient communication mechanisms [51, 76]. Nevertheless, wireless communication remains a major barrier to the overall sustainability of embedded deployments.

Wireless communication is the most power-intensive task performed by embedded devices, consuming at least an order of magnitude more power than sensing and processing [40, 75]. This arises from the need to generate and amplify radio waves [23, 45], which involves power-hungry analog components such as oscillators, amplifiers, and mixers. Transmission, in particular, consumes more power than reception because of its dependence on amplifiers to produce strong signals. Since embedded systems generally transmit more frequently than they receive, mitigating the cost of transmissions could substantially reduce the overall power consumption.

Backscatter transmitters have emerged as a promising approach, attracting significant research interest in the past decade [23, 40, 45, 75, 81]. Although not new–first demonstrated over half a century ago and widely used in RFID tags–backscatter has recently seen renewed interest in enabling applications beyond traditional RFIDs. Backscatter transmitters reduce power consumption by shifting energy-intensive analog tasks away from the transmitter. This allows the transmitter to focus solely on low-power baseband processing and digital tasks. The necessary carrier signals can come from powerful devices such as readers and routers, or even ambient signals [45, 75, 81, 84]. However, despite numerous advances, backscatter has seen slower adoption than expected. This raises an important question: *What has prevented the widespread deployment of backscatter transmitters despite the significant potential to enable sustainable embedded deployments ?*

Several challenges have hindered the broader adoption of backscatter transmitters. In particular, they often require dedicated carrier emitter devices, which must typically be placed in close proximity to the tags, a constraint that limits deployment [81]. Although some approaches attempt to leverage ambient signals, they face significant limitations, particularly in indoor environments where weak ambient signals, combined with the inherent losses of the backscatter process, lead to impractically short ranges [45, 88]. Furthermore, operating in shared wireless spectrum introduces additional complications. Inherently weak backscattered signals are highly susceptible to interference from more powerful coexisting devices, resulting in packet loss, latency, and reduced reliability.

Design. We present AudioCast to address both the spectrum and energy challenges in embedded systems. The key contribution of AudioCast is the conceptualization of a novel transmitter architecture, Beyond-Backscatter (BB) Transmitter that moves beyond the limitations of backscatter mechanisms by eliminating the need for carrier

Table 1. Comparison of AudioCast with existing backscatter and low-power transmitters. The AudioCast transmitter can reliably transmit up to 130 m while maintaining overall power consumption below 200 µW.

System	External Carrier	Frequency (MHz)	Range (m)	Power (µW)	Bit Rate (bps)	Speech Quality
FM Backscatter [88]	Ambient carrier	88 – 108	6	11.07	3.2k	PESQ ≈ 2
FM Backscatter [34]	Ambient carrier	88 – 108	19.6	150	1k	NA
Judo [84]	Carrier emitter (>100 m)	868	100	100	100k	NA
TunnelRadio [64]	Not required	88 – 108	24	150	NA	NA
AudioCast	**Not required**	**88 – 108**	**130**	**200**	**368 – 10.7k**	**PESQ > 1.29**

emitter devices. It addresses spectrum scarcity by using the unoccupied FM-broadcast band and using existing broadcast radio receivers for communication. AudioCast broadcasts information as audio messages. Although built from standard components, the AudioCast transmitter operates at power levels below 200 µW– comparable to the state-of-the-art backscatter transmitters [81], as shown in Table 1.

The BB-Transmitter builds on recent advances in using tunnel diodes to design low-power oscillators [49, 80, 83, 84], enabling carrier signal generation with power consumption below 200 µW and bias voltages under 200 mV. However, tunnel diode oscillators (TDOs) often trade stability for low-power operation [78, 84], leading to challenges such as frequency drift caused by nearby motion, environmental changes [80, 84], or even subtle effects such as a person's breathing [78]. To overcome these issues, we systematically addressed the sources of instability and incorporated targeted design enhancements into the BB-Transmitter architecture.

We systematically studied the factors that contribute to instability in TDOs. First, we found that TDOs exhibit improved stability at lower frequencies. Second, the biasing network plays a critical role; designing a practical biasing circuit is challenging due to the non-linear behavior of the diode. We observed that using a regulated power supply combined with a diode network significantly improves stability by maintaining the tunnel diode within its negative resistance region while stepping down a higher supply voltage. To mitigate the influence of electromagnetic interference, both from the transmitter and from nearby sources [78]—we integrated a diode network, an RF isolator and an EMI shielding box into the BB-Transmitter design. Together, these design choices effectively stabilize the TDO, even in the presence of nearby movement, thus eliminating the need for an external carrier emitter device for injection-locking [84].

We address the challenge of contention by purposefully transmitting information over the FM-broadcast band (88—108 MHz). This spectrum offers superior propagation characteristics that enable long-range communication at low transmit power. While FM-radios remain prevalent in some regions, they are being phased out in others, and many modern smartphones no longer include FM-receivers. This trend creates an opportunity to reuse the FM-broadcast band for embedded communication. The feasibility is further supported by off-the-shelf radio chipsets that support this frequency band. Additionally, regulations in many countries permit unlicensed use of the FM-broadcast band, provided transmissions stay within defined power limits. AudioCast promotes the use of this underutilized spectrum for embedded systems, particularly due to the relative scarcity of interfering emitters in this band. Since available frequencies vary by region, we also discuss the challenges of dynamic spectrum selection and provide tools to help users identify unallocated FM channels based on their geographic location.

FM-radio receivers typically rely on analog modulation techniques, such as frequency and amplitude modulation. In this work, we demonstrate a unique property of the TDO, which we refer to as self-modulation. This property enables us to frequency modulate the carrier signal directly using the TDO without the need for external and power-consuming modulating and mixing circuits. We systematically investigate how the frequency and amplitude of the baseband signal influence the modulation index.

Most applications require the deployment of multiple tags within an environment, necessitating a mechanism for co-existence and efficient spectrum utilization. To address this, we develop a frequency-division multiple

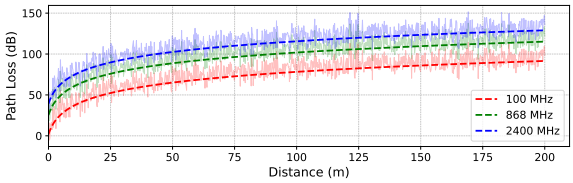

Fig. 2. Radio-wave propagation loss decreases significantly at lower frequencies, particularly in the FM-broadcast band (88–108 MHz). This reduction in path loss enables long-range wireless communication even at a low transmit power.

access (FDMA)-based scheme that assigns separate channels to each tag. In addition, we conducted detailed experiments to demonstrate the feasibility of simultaneous transmissions from multiple tags while maintaining reliable communication. Putting these contributions together, the highlights of the results are as follows:

Summary of results.

- AudioCast achieves a range of up to 130 m in line-of-sight (LoS), 110 m in mixed LoS, and tens of meters in non-line-of-sight (NLoS) environments—all without requiring a carrier emitter device.
- AudioCast demonstrates the self-modulation property of TDO, which allows the frequency modulation of TDO without additional circuits. This allows reception via ubiquitous FM-receivers. AudioCast maintains intelligible speech quality, achieving PESQ scores greater than 1.29.

Application use cases. We prototype and demonstrate three novel use cases enabled by AudioCast's unique properties: (1) a wearable device that transmits voice data from individuals at µW-scale power consumption, (2) communication of hand gesture information for scenarios such as appliance control, and (3) backhauling information to support city-wide sensor deployments.

2 Background

We provide background on the system's design: *First*, we analyze the benefits of using a lower-frequency spectrum for wireless connectivity. Next, we contrast the advantages of FM-broadcast spectrum with TV-whitespace, which uses unused UHF spectrum. *Finally*, to contextualize our approach, we review related work on low-power transmitter design, including systems based on backscatter mechanisms and tunnel diode-based architectures.

2.1 Lower-Frequency Enables a Long Communication Range

Wireless communication range is dependent on the operating frequency. Lower frequencies exhibit superior propagation characteristics, thus supporting longer-range communication even at lower transmission power. For instance, free-space path loss scales with the square of frequency (Friis' equation), making sub-1 GHz bands *10–100*× more power-efficient than 2.4 or 5 GHz ISM bands. In addition, lower-frequency signals also penetrate obstacles such as walls more effectively, making them ideal for NLoS deployments and dense urban environments.

Broadcast radio and television systems, for example, FM-broadcast (≈ 88–108 MHz) and UHF TV (≈ 470–698 MHz), exploit low-frequency propagation properties to sustain kilometers-scale links. AudioCast's tunnel-diode oscillator, operating at microwatt-level power, leverages the FM-broadcast band to enable long-range communication. To quantify this capability, we applied the Extended Hata (eHata) model [2], which has been validated for frequencies ranging from 30 to 3000 MHz in various environments. The simplified path-loss expression is:

$$p_L(f, H_m, H_b, d, env) = L(f, H_m, H_b, d, env) + T(G(\sigma))) \tag{1}$$

Here, H_m and H_b denote the minimum and maximum antenna heights (set to 1 when <1 m from ground), L is the median path loss, σ is the shadowing standard deviation, f is frequency, d is the TX-RX distance and env indicates the environment (urban, suburban, or rural). Figure 2 shows the simulated path loss across frequencies using eHata. Solid lines denote mean loss, while shaded regions show deviation due to shadowing and multipath

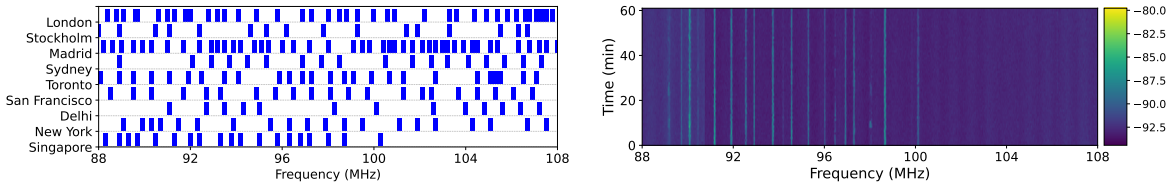

(a) FM radio stations across major cities

(b) One-hour spectrum of local FM-broadcasts

Fig. 3. Frequency allocation for radio stations within the FM-broadcast spectrum (88–108 MHz) remains sparse across major cities worldwide, as illustrated by the blue bars. Despite the FM-broadcast spectrum's favourable propagation characteristics and regulatory allowances for unlicensed transmissions, a significant portion remains unallocated and underutilized. Our one-hour spectral measurement of the FM-broadcast band at our location further confirms this under-utilization.

effects. We observe that at 100 MHz, the path loss is at least 25 dB lower than at 2.4 GHz—over 300× lesser power loss. This allows AudioCast to combine sub-200 µW power with over 100 m range, consuming at least 10× lesser power consumption than commercial transceivers, which achieve a similar communication range and bitrate.

2.2 Television and FM-broadcast Spectrum

Repurposing unoccupied television spectrum—commonly referred to as "whitespaces"—has emerged as a promising approach for networking in embedded systems [9, 12, 67]. This opportunity arises due to the shift from over-the-air television broadcasts to internet streaming, freeing up sub-1 GHz spectrum for computer communication. The television spectrum is attractive for several reasons. *First*, lower-frequency (sub-1 GHz) allow for compact, reasonably sized yet efficient antennas. *Second*, lower-frequency offer superior propagation, allowing radio-waves to penetrate walls and travel several times farther than 2.4/5 GHz signals, particularly NLoS. *Finally*, operating in the TV bands avoids cross-technology interference with protocols such as Wi-Fi and Bluetooth. Consequently, regulators in many countries allow unlicensed transmission in unoccupied TV spectrum.

Television-broadcast spectrum. Terrestrial television broadcasts occurs on the 54–806 MHz band, with 6 MHz allocated per channel in the very high frequency (VHF; 54–88, 174–216 MHz) and ultra-high frequency (UHF; 470–806 MHz) bands, and vary by region. With the global shift to digital and internet-based television services, much of this spectrum has become available for licensed and unlicensed computer communication [26, 35].

FM-broadcast spectrum. FM broadcasts occur in the lower-frequency spectrum (below 108 MHz). We surveyed frequency allocations in ten major cities to assess the potential of FM-broadcast bands as whitespaces for computer communication. As shown in Figure 3(a), our analysis reveals that a significant portion of FM-broadcast spectrum remains unallocated [19, 24, 25, 48, 58, 59]. We also conducted a study using a spectrum analyzer (BB60C from SignalHound [33]) at our location (Figure 3(b)), which confirms this sparsity, further underscoring the under-utilization of the FM-broadcast spectrum. In addition, countries such as Norway and Switzerland have already phased out FM broadcasts in favour of digital services [74, 92], further supporting our argument.

Although the FM-broadcast spectrum offers promising opportunities for unlicensed communication, it also introduces the challenge of selecting appropriate frequencies. These unoccupied bands must be regionally selected, potentially requiring re-tuning when relocated to a different geographic area. AudioCast can leverage community-maintained databases [60] to identify occupied channels and dynamically adjust transmission frequencies. Alternatively, scanning with low-power envelope detectors [45] can help avoid active stations. To further simplify frequency selection during deployment, we provide a script[1] that identifies unallocated frequencies based on device location, using publicly available sources to build a database of allocated channels. We make this repository open to contributions to help expand and maintain the database.

[1] https://github.com/weiserlab/AudioCast/tree/main/frequency_scanner

Finally, FM broadcasts are licensed; regulations, such as FCC Parts 15.231 and 15.239 [22, 27], permit low-power, unlicensed transmissions. For continuous transmissions with a bandwidth ≤ 200 kHz, the specified communication range is approximately 61 m, corresponding to a field strength of 250 μV m^{-1} at 3 m. For periodic transmissions, the service range may extend beyond 160 m, with an allowable field strength of 500 μV m^{-1} at 3 m. AudioCast transmissions, due to the inherently low-power nature of tunnel diodes, result in weak emissions and easily comply with these regulatory constraints. AudioCast also builds on the sparsity of the FM-broadcast spectrum.

2.3 Low-power Transmitters based on Backscatter Mechanism

RFID is one of the most widely deployed embedded systems, leveraging backscatter communication with billions of tags worldwide [91]. Although RFID enables battery-free operation, its use in sensing applications is limited by several factors: the energy-intensive reader infrastructure [81], short communication ranges (typically under 10 m), and challenges in adapting the system to custom sensing applications [89].

Over the past decade, efforts have been made to overcome RFID limitations and apply backscatter to embedded applications. There have been efforts to decouple the backscattered signal from the carrier signal in frequency to mitigate self-interference [95]. Building on this approach, subsequent work has enabled the generation of baseband signals compatible with commodity protocols, such as Wi-Fi [38], Bluetooth [23], and ZigBee [37, 56]. This enabled reception on commodity devices, such as smartphones and laptops, eliminating the need for RFID readers. However, these systems require the tag to be in proximity to the carrier emitter device, which limits the deployment scenario. Efforts have also explored trading off bitrate for sensitivity to extend the communication range of backscatter systems. In particular, LoRa-based backscatter mechanisms achieve hundreds of meters of range while operating at μW-scale power consumption [55, 75]. Varshney et al. extend the range of the backscatter mechanism [81] to kilometers while reducing the cost of both the carrier emitter device and receiver.

Despite these advances, backscatter systems still rely on carefully positioned carrier emitter devices to illuminate tags with carrier or excitation signals [40, 81]. This requirement limits the flexibility and practicality of deployments. AudioCast overcomes this constraint through its BB-transmitter architecture, which achieves a power consumption comparable to backscatter tags, while eliminating the need for a carrier emitter device. By operating in the underutilized FM-broadcast spectrum, AudioCast also avoids interference challenges that often affect weak backscatter signals in congested ISM bands (e.g., Wi-Fi/BLE crosstalk). This combination of carrier emitter device-free operation and spectral efficiency enables novel applications in environments and scenarios where traditional backscatter systems face limitations, as demonstrated by the experiments in this work.

2.4 Backscattering using Ambient Wireless Signals

Efforts have been made to design transmission mechanisms that operate without a carrier emitter device. Ambient backscatter leverages ubiquitous wireless signals, reflecting or absorbing them to communicate with specialized receivers. Liu et al. pioneered this concept by demonstrating its feasibility using television signals [45]. Based on this work, Kellogg et al. [38] and Zhang et al. [93] utilized Wi-Fi signals. However, ambient signals in urban environments face coverage limitations. To address this, FM backscatter systems [13, 14, 87, 88] take advantage of the superior propagation characteristics and wide coverage of FM broadcasts. Wang et al. demonstrated the feasibility of backscattering ambient FM signals, enabling commodity smartphones to receive transmissions [88]. Daskalis et al. used FM backscatter to transmit temperature data in agricultural deployments [13, 14], while Hu et al. [34] designed an FM backscatter tag that incorporates a tunnel diode reflection amplifier to improve range. However, all of these approaches are based on the presence of ambient FM signals, which are being phased out in several regions. More generally, the backscatter mechanism suffers from significant signal strength loss (often exceeding 30 dB) [83], which severely limits the range unless the tag is placed very close to a strong transmission source, such as a radio tower, as also confirmed by the experiments presented in this work.

2.5 Tunnel Diodes

Tunnel diodes are semiconductor devices characterized by a heavily doped p-n junction, with doping levels of orders of magnitude higher than those of conventional diodes [70]. This extreme doping creates an ultra-thin depletion region, enabling quantum tunneling and resulting in distinctive current-voltage (I-V) characteristics. As depicted in Figure 5(b), tunnel diodes exhibit a negative resistance region: once the forward voltage exceeds a critical threshold (typically tens of mV), the current decreases with increasing voltage. This phenomenon occurs at low bias voltages (tens to hundreds of μV) and currents (a few mA), allowing operation on the μW scale.

Reflection amplifiers. Tunnel diodes have been used to enhance backscatter systems by designing reflection amplifiers. Amato et al. demonstrated a 5 GHz tag integrating a tunnel diode reflection amplifier, achieving 40 dB gain [5], while Varshney et al. extended this to 868 MHz with 34 dB gain [80, 83]. GPSMirror leveraged tunnel diodes to amplify weak GPS signals and relay them indoors [18], and Hu et al. developed an FM-backscatter tag using tunnel diodes for long-range ambient backscatter transmission [34]. Although these systems achieve microwatt-level power consumption, they depend on ambient or dedicated carrier signals from carrier emitter devices. This makes deployment complex and increases contention in the ISM band due to strong carrier signals. AudioCast tackles these limitations with its BB-transmitter architecture, eliminating the need for a carrier emitter device. Furthermore, the system also demonstrates the self-modulation property of tunnel diode oscillators.

Transmitters. AudioCast builds on recent efforts to move beyond backscatter architecture by designing transmitters using tunnel diode-based oscillators. TunnelScatter demonstrated that a tunnel diode transmitter could operate without a carrier signal using On-Off Keying (OOK) modulation [83]. Judo introduced the self-oscillating mixing property of tunnel diode oscillators, achieving high transmission range and bitrate [84]. TunnelEmitter used a tunnel diode oscillator to implement a standalone carrier emitter [80], while TunnelLiFi applied it to build a light sensor [49]. Each of these systems faced challenges stemming from the inherent instability of tunnel diodes, particularly the frequency drift in the oscillator caused by nearby motion. Thaddeus et al. leveraged this instability to design a low-power sensor for monitoring vital signs [78]. AudioCast introduces the BB-transmitter architecture, which mitigates the frequency drift of tunnel diode oscillators and enables deployments without a dedicated carrier emitter device. Furthermore, AudioCast is the first to demonstrate the frequency modulation capability of tunnel diode oscillators, which we refer to as self-modulation, allowing for audio broadcasts compatible with commodity FM radio receivers, such as those found in cars and phones.

AudioCast is most closely related to, and builds upon, TunnelRadio [64], but significantly advances beyond its design. *First*, we introduce techniques to stabilize the tunnel diode oscillator, addressing TunnelRadio's susceptibility to frequency drift, a shortcoming that, as shown in our motion experiments, severely impacts communication reliability in mobile scenarios. *Second*, we employ an FSK-like modulation scheme that encodes sensor data as audio tones, allowing reliable demodulation by commodity FM receivers. In contrast, TunnelRadio uses unmodulated carriers, which cannot convey sensor information. *Third*, AudioCast supports concurrent transmissions using FDMA. *Fourth*, we extend the communication range to over 100 m, achieving a 5× improvement over TunnelRadio, as shown in Table 1. *Fifth*, we demonstrate and evaluate the self-modulation property of the tunnel diode oscillator. *Finally*, we prototype real-world applications to demonstrate the practicality of the system.

2.6 Motivation for going Beyond-Backscatter Transmitters

Backscatter [23, 40, 75, 81], reflection amplifiers [5, 21, 83], and tunnel diode transmitters [49, 84] address energy challenges in embedded systems by enabling low-power transmissions and balancing power consumption between sensing, processing, and transmission tasks. However, all of these approaches share one common limitation: the need for a carrier emitter device. Backscatter and reflection amplifiers operate by reflecting or absorbing the carrier signal, whereas tunnel diode-based transmitters, such as Judo [84], rely on them for injection locking. This dependence restricts the applicability of such systems, as the precise placement of the emitter device may

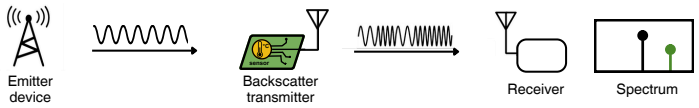

(a) Ambient backscatter system

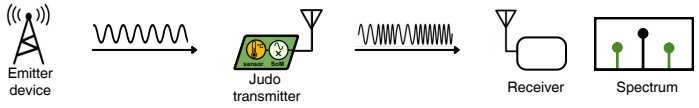

(b) Injection-locked tunnel diode transmitter

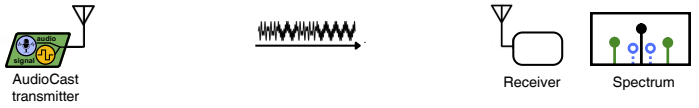

(c) AudioCast system

Fig. 4. The BB-Transmitter enables the AudioCast system. Due to several design choices, AudioCast avoids the need for a carrier emitter device. This provides deployment flexibility over injection-locked TDO and backscatter transmitters.

not always be practical or feasible in real-world deployments. Hence, there is a need to design transmission mechanisms that avoid a device such as a carrier emitter device while preserving the low-power characteristics of the backscatter mechanism. The BB-transmitter architecture of AudioCast precisely addresses this challenge.

In particular, several efforts have been made to design transmitters that avoid the carrier emitter device. They generate carrier signals locally, minimizing radiated power for low-power operation. One of the first systems, presented in 1963 [41], described a tunnel-diode-based FM transmitter for medical research and laboratory telemetry. However, it was not designed to transmit digital information and had a relatively high power consumption of approximately 1.6 mW. More recent efforts have used tunnel diode oscillators to design transmitters that support on-off keying (OOK) modulation [83] or as emitter devices [80] for backscatter tags; however, these designs have faced stability challenges. AudioCast builds on these previous works and addresses the limitation of instability.

3 Design

We present AudioCast transmitter, conceptualizing the **Beyond-Backscatter (BB)** architecture and focusing on a few key aspects of the architecture. *First*, we analyze the impact of the operating frequency on the stability of the TDO. *Second*, we explore design choices to enhance oscillator stability without relying on the injection locking mechanism. *Third*, we introduce and leverage the self-modulation property of the TDO to frequency-modulate the carrier signal directly, eliminating the need for external modulation circuits. *Fourth*, we detail the communication scheme, which encodes information as audio tones broadcast by the tunnel diode oscillator. *Finally*, we demonstrate AudioCast's support for multiple transmitting tags, enabling scalable deployments.

3.1 Beyond-Backscatter Architecture

AudioCast implements the BB-Transmitter architecture taking advantage of the underutilized FM-broadcast spectrum (88–108 MHz). By encoding data as frequency modulated signals, AudioCast enables reception on ubiquitous FM-receivers found in cars, smartphones, and home devices, without the need for specialized receivers or hardware modifications. Figure 1 presents an overview of the AudioCast, while Figure 4 compares the BB-Transmitter architecture with other low-power transmitter architectures.

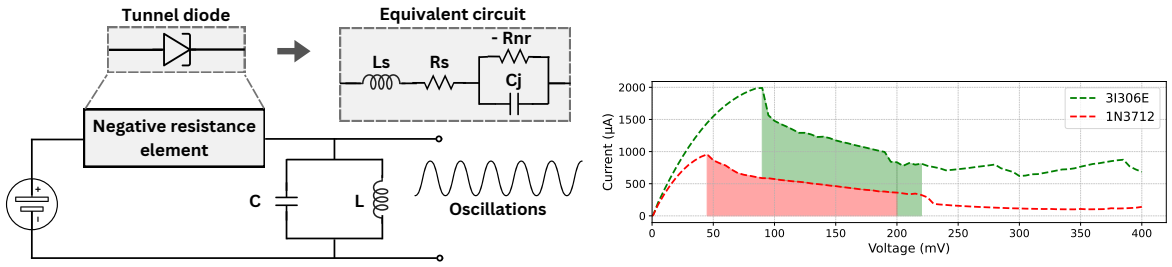

(a) Oscillator designed using negative resistance

(b) I-V characteristic of tunnel diodes

Fig. 5. An oscillator fundamentally consists of a negative resistance element coupled with a resonant circuit. The oscillation frequency depends on the characteristics of both the negative resistance element and the resonant circuit. Tunnel diodes are an ideal negative resistance element due to their nonlinear current-voltage characteristics, including a distinctive voltage-dependent negative resistance region. The equivalent circuit of a tunnel diode includes the negative resistance (R_{nr}) in parallel with the junction capacitance (C_j). Additionally, parasitic elements—such as the inductor (L_s) and the resistor (R_s) from connecting leads—are incorporated into the model to account for real-world behavior.

Generating a carrier signal. A carrier signal is generated using an oscillator, which is usually designed by coupling a negative resistance element with a resonant circuit (Figure 5(a)). Although transistors are commonly used as the negative resistance element, they often require higher power consumption and operating voltages. The BB-Transmitter builds on recent work showing that carrier signal generation, historically considered energy-intensive, can now be achieved with power consumption as low as tens of μW using tunnel diodes.

Based on previous efforts [21, 49, 80, 83, 84], we designed a tunnel diode oscillator (TDO) consisting of an inductor, a capacitor, and the inherent parasitics of the antenna and the PCB as resonant elements, with the tunnel diode serving as the negative resistance component. We configured the TDO to generate carrier signals in the FM-broadcast band by fine-tuning the resonant circuit parameters. Specifically, we targeted the FM band ranging from 88 MHz to 108 MHz and designed the TDO using 3I306E and 1N3712 tunnel diodes.

Nonetheless, the design of the TDO involves several trade-offs to achieve low power consumption: it generates a weak radiated signal, exhibits higher phase noise, and suffers from frequency instability. Thaddeus et al. [78] even leveraged this instability to monitor vital signs such as breathing. However, these limitations pose challenges for transmitter design, where stable carrier frequency and strong signal strength are desirable to ensure reliable link quality. Hence, we describe several design choices made in BB-Transmitter to address these concerns.

3.1.1 Design Choice 1: Operating at Low-frequency. The frequency of a TDO is influenced by various factors, including environmental conditions like temperature fluctuations, humidity [80], and nearby motion [78]. Furthermore, the presence of external RF signals can also cause instability. The TDO frequency also drifts naturally over time. We aim to mitigate frequency drift while preserving the low-power characteristics of the TDO.

Understanding the stability of TDO. Let us look at the stability criteria of the TDO. We used the equivalent small signal model for the tunnel diode [70] to understand the stability conditions for tunnel diode oscillators. The operating frequency is dependent on the LC tank circuit. In Figure 5(a), the tunnel diode can be replaced by its equivalent circuit. The effective negative resistance is dependent on the shunting effect of the intrinsic junction capacitance. The effective negative resistance can be derived [29] as:

$$R_{nr}{}' = \frac{R_{nr}X_c^2}{X_c^2 + R_{nr}^2} \tag{2}$$

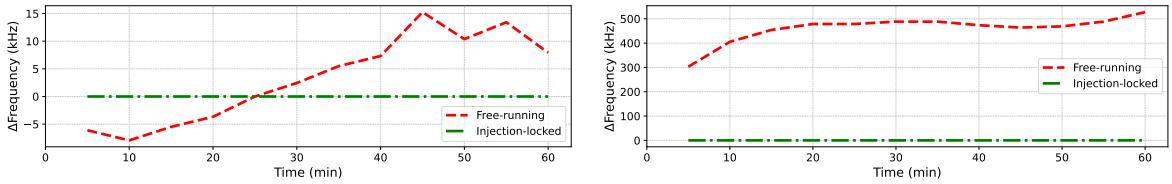

(a) FM-broadcast band

(b) 800-900 MHz band

Fig. 6. A free-running TDO exhibits significant frequency drift, often deviating by hundreds of kilohertz from its nominal frequency. Injection locking the TDO using an external carrier signal can stabilize the frequency and eliminate this drift; however, this approach requires introducing one or more carrier emitter devices into the deployment.

where, $R_{nr}{}'$ is the effective negative resistance, R_{nr} is the negative resistance of the tunnel diode and X_c is the ac reactance of the junction capacitance C_j. If we consider that the tunnel diode is operating at the frequency f, we have $X_c = \frac{1}{2\pi f C_j}$, which on substituting and simplifying the previous equation we get,

$$R_{nr}{}' = \frac{R_{nr}}{(2\pi f C_j R_{nr})^2 + 1} \tag{3}$$

With an increasing operating frequency of the oscillator, the effective negative resistance is reduced, which is necessary for sustained oscillations. Furthermore, the condition for the stability [29, 50] is given by,

$$\frac{L_T}{|R_{nr}{}'|C_j} < R_T < |R_{nr}{}'| \tag{4}$$

Where, L_T and R_T are the values of the inductance and resistance of the lump circuit (including the parasitic inductances and resistances). With decreasing negative resistance, the above inequality becomes tighter, and the condition for stability becomes more difficult to achieve. This also reduces the allowed variation of parasitic components and their increased effect on the stability and frequency of the TDO.

Injection-locking. One mechanism for stabilizing the TDO carrier frequency is the injection-locking [49, 84] phenomenon. This occurs when two oscillators with close resonant frequencies are coupled, causing them to oscillate in unison. The minimum signal strength of the carrier required for injection lock is dependent on the frequency difference between the resonant frequency of the TDO and the external carrier. It is proportional to the minimum injection current needed to alter the frequency, which is represented by the equation:

$$I_i \approx 2QI_o\frac{|f_0 - f_c|}{f_0} \tag{5}$$

Where I_i is the minimum injection current, Q is the quality factor, f_0 is the oscillator frequency, and f_c is the external carrier signal frequency. We used the injection-locked oscillator as a baseline to compare the stability with a free-running oscillator in Figure 6, and it shows the lower drift in the frequency of the carrier signal generated by the oscillator due to injection locking. However, we aim to eliminate the need for an emitter device. Next, we detail our choices and the methods used to stabilize the TDO without relying on injection locking.

Low-frequency leads to improved stability. From the above analysis, we conclude that operating at lower frequencies improves the stability of the TDO. We empirically show this experimentally by comparing the stability of TDOs across different frequency bands. In one setup, we configured a TDO to operate within the FM-broadcast band and connected it to an antenna. A nearby spectrum analyzer monitored the emitted signal over one hour. We repeated the same experiment with a TDO tuned to a frequency near the 868 MHz band. In both cases, we also evaluated the stability under injection-locking using an external carrier signal.

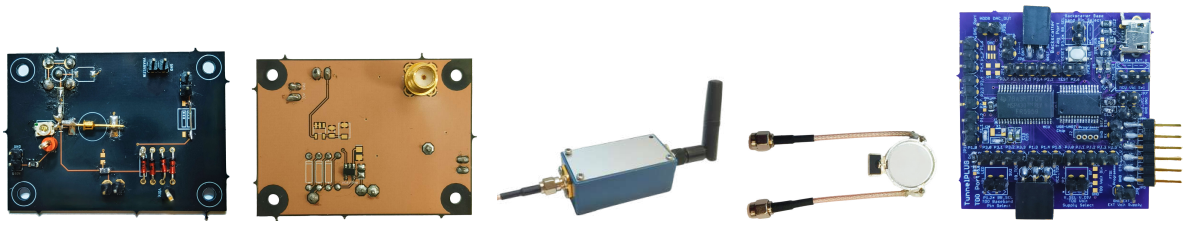

(a) Frontend (front view) (b) Frontend (back view) (c) EMI shielded casing (d) Isolator (e) Baseband generator

Fig. 7. AudioCast hardware prototypes

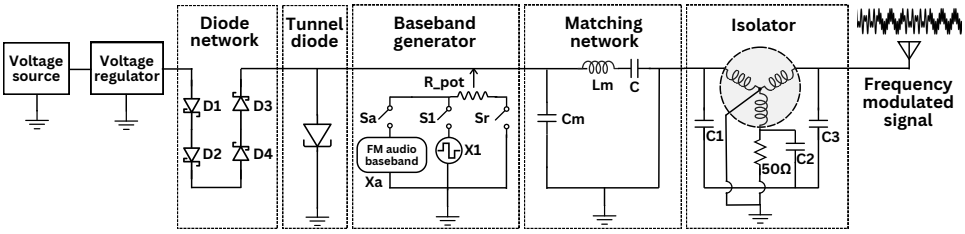

Fig. 8. A BB-Transmitter integrates a tunnel diode with a resonant circuit to generate a carrier signal locally. To maintain stable resonant frequency, a biasing circuit ensures the tunnel diode remains in its negative resistance region, also preventing frequency fluctuations due to voltage changes. An RF isolator further enhances the stability of TDO by blocking radio-waves.

Figure 6 shows the result of the experiment, in which the TDO operating in the FM-broadcast band demonstrated better stability. The difference in stability between the free-running and injection-locked configurations at this lower frequency was minimal. Specifically, the free-running oscillator exhibited a frequency drift of only a few kilohertz (around ±15 kHz) from its set frequency. In contrast, the TDO operating at the higher frequency showed a significant frequency drift of several hundred kilohertz (around ±0.5 MHz).

3.1.2 Design Choice 2: Improving the bias circuit. A biasing circuit ensures that the tunnel diode remains within its negative resistance region by maintaining a precise bias voltage. TDOs present unique challenges for such circuits. *First*, even minor changes in bias voltage can cause significant frequency drift. Our experiments show that a mere variation 1 mV can shift the TDO frequency by hundreds of kilohertz. This is due to the highly non-linear nature of tunnel diodes, where slight changes in voltage alter their effective negative resistance, internal capacitance, and inductance. *Second*, the negative resistance region of a tunnel diode begins at low voltages—typically tens of millivolts—while baseband and associated circuits often operate at much higher voltages, around 1.8 V. *Finally*, because of the self-oscillating mixing and self-modulation properties of TDOs, they are prone to interference from unwanted noise or emissions, which can mix with the generated radio signals and degrade performance.

We designed a biasing circuit to address these challenges. To achieve the required voltage drop from a higher voltage rail while minimizing energy waste, we used very low forward-voltage, low-resistance barrier diodes connected in series. This configuration also provides isolation from the rest of the circuit, preventing noise from interfering with the TDO. Furthermore, we observed that the diode network enhances the stability of the TDO, reducing the frequency drift caused by nearby motion. A low-power voltage regulator supplies a steady bias voltage of 1.2 or 1.3 V. These design elements are shown in the schematic of the BB-Transmitter in Figure 8.

3.1.3 Design Choice 3: Isolators and EMI shielding. TDOs are highly sensitive to changes in their electromagnetic environment [78], which can cause frequency drifts. Ensuring TDO stability requires isolating the oscillator from the RF load to prevent frequency shifts, loading effects, and instability due to impedance variations. In RF systems, any mismatch between the oscillator and the load can result in signal reflections that feed back into the TDO, disrupting its operation and leading to instability or signal distortion. To mitigate these effects, we incorporate

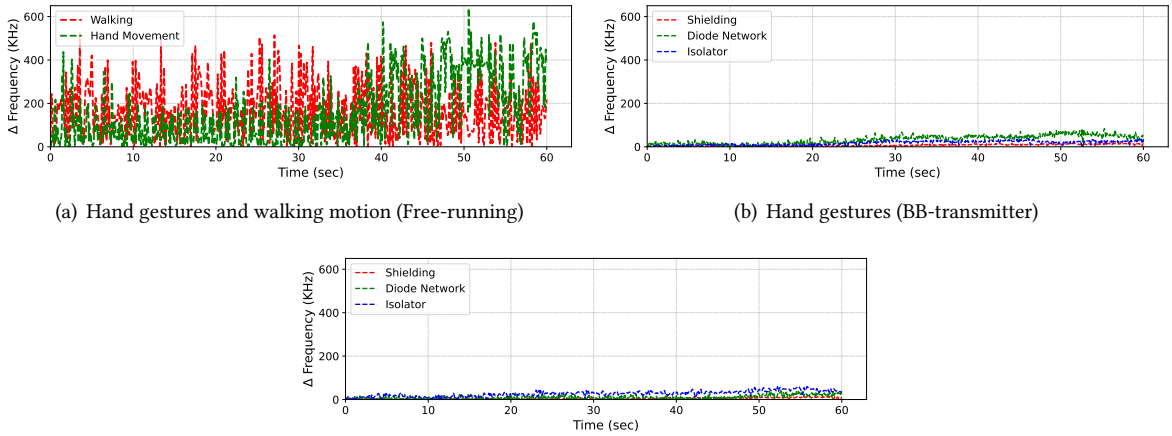

(a) Hand gestures and walking motion (Free-running)

(b) Hand gestures (BB-transmitter)

(c) Walking motion (BB-transmitter)

Fig. 9. A free-running TDO exhibits significant frequency drift in the presence of nearby movement, such as hand motion or walking, making it unsuitable for communication. By incorporating measures like EMI shielding, an RF isolator, and a bias circuit, BB-Transmitter significantly enhances the TDO's stability, resulting in improved link quality for communication.

an RF isolator and an EMI shielding box. These components help prevent reflected signals from interfering with TDO and reduce the influence of external electromagnetic noise. We illustrate this configuration in Figure 8.

Putting everything together. Through a combination of design choices, including a dedicated diode network, a voltage regulator, operation at lower frequencies (particularly within the FM-broadcast band), and the use of an RF isolator and EMI shielding, we successfully stabilize the TDO without relying on injection locking. These improvements enable the realization of the BB-transmitter, as illustrated in Figures 7 and 8.

Figure 9 illustrates the improved stability of the TDO. Within the FM-broadcast band, the TDO exhibits minimal drift as shown in Figure 6. To demonstrate the benefits of our design, we present results for the TDO operating at 868 MHz, where comparable stability is observed. We conducted this experiment in a controlled university laboratory environment, placing the transmitter on a table, making hand gestures, and walking around it for approximately 1 minute. A spectrum analyzer placed 1 m away recorded the TDO frequency drift. The frequency drift of the unstable free-running TDO reached about 600 kHz, as seen in Figure 9(a). In contrast, our design significantly reduces this drift by almost an order of magnitude, as demonstrated in Figures 9(b) and 9(c). Figure 10 presents the frequency drift of the TDO over an extended period of 1 hour. We conducted experiments in two environments: a controlled closed-room setting and a dynamic laboratory environment with external activity and surrounding interference. In both cases, the transmitter was powered by a CR2023 3 V coin-cell battery. A spectrum analyzer positioned 1 m away recorded the frequency of the TDO over time through multiple iterations. Our results show that the diode network played a more significant role in stabilizing the TDO than the isolator and the EMI shielding, as shown in Figures 10(b) and 10(c). These findings confirm that, through a combination of targeted design choices, we have successfully stabilized the TDO.

3.2 Modulation

To transmit information, the generated carrier signal must be modulated. Conventional transmitters typically rely on energy-intensive components, such as mixers, which we aim to avoid in the BB-Transmitter. Previous works like Judo [84] and TunneLiFi [49] have shown that a TDO exhibits a self-oscillating mixing (SoM) property, allowing it to mix a weak baseband signal with the TDO output. However, to preserve compatibility with

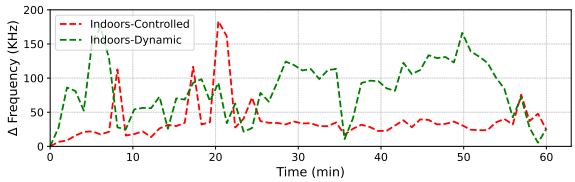

(a) Free-running

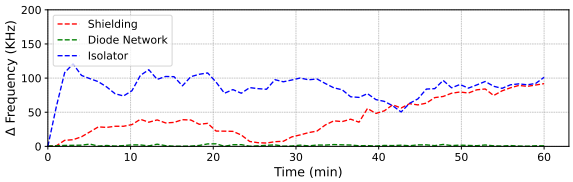

(b) Controlled environment, BB-transmitter

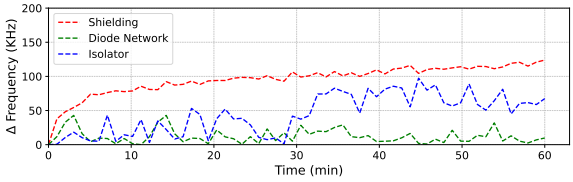

(c) Uncontrolled environment, BB-transmitter

Fig. 10. Natural frequency drift refers to variations in the TDO's frequency when the transmitter operates in an uncontrolled environment. The BB-transmitter architecture, particularly its biasing network, significantly reduces this drift.

commodity FM-receivers, it is necessary to apply frequency modulation (FM) directly to the carrier. Unlike SoM, which produces intermodulation products, direct FM modulation varies the carrier frequency according to the baseband signal. To enable this, we demonstrate a distinct property of the TDO: *self-modulation.*

FM-modulation primer. As the name suggests, FM radio broadcast stations use frequency modulation to transmit information. In frequency modulation, the message signal is encoded as a deviation of the carrier wave. A frequency modulated signal [31] can be represented as,

$$s(t) = A_c cos[2\pi f_c t + 2\pi k_f \int_0^t m(\tau) d\tau] \tag{6}$$

where, A_c and f_c are the amplitude and frequency of the carrier signal, k_f is the sensitivity factor of the modulator (Hz/ V) and m is the message signal. For a sinusoidal message signal $m(t) = A_m cos(2\pi f_m t)$, we get

$$s(t) = A_c cos[2\pi f_c t + \frac{\Delta f}{f_m} sin(2\pi f_m t)] \tag{7}$$

Here, $\Delta f = k_f A_m$ is the maximum frequency deviation of the carrier and the fraction $\frac{\Delta f}{f_m}$ is the modulation index denoted by β. Depending on the value of β, we can define the modulation to be either narrowband frequency modulation for very small values ($\beta << 1$) or wideband frequency modulation for larger values. The Eq. 7 can be expanded using the trigonometric identity $cos(A + B) = cos(A)cos(B) - sin(A)sin(B)$ giving,

$$s(t) = A_c cos(2\pi f_c t) cos[\beta sin(2\pi f_m t)] - A_c sin(2\pi f_c t) sin[\beta sin(2\pi f_m t)] \tag{8}$$

For the specific case of narrowband frequency modulation with $\beta << 1$, we can approximate $cos[\beta sin(2\pi f_m t)] \approx 1$ and $sin[\beta sin(2\pi f_m t)] \approx \beta sin(2\pi f_m t)$, resulting in $s(t) \approx A_c cos(2\pi f_c t) - A_c \beta sin(2\pi f_c t) sin(2\pi f_m t)$. Further expanding this equation using $sin(A)sin(B) = \frac{1}{2}[cos(A + B) + cos(A - B)]$,

$$s(t) \approx A_c cos(2\pi f_c t) - \frac{1}{2} A_c \beta [cos(2\pi (f_c + f_m) t) - cos(2\pi (f_c - f_m) t)] \tag{9}$$

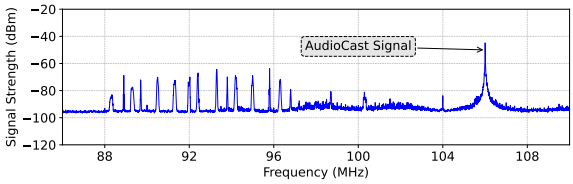

Fig. 11. AudioCast generates transmissions within the FM-broadcast band (88–108 MHz). We center the signal at 106.1 MHz, a frequency unoccupied in our location, to avoid interference with existing FM-radio stations. The figure shows the spectrum, highlighting both ambient FM-broadcast and AudioCast 's transmission with a post-propagation strength of -44 dBm.

In Eq. 9, if we consider only the last two terms, a narrow band frequency modulated signal can be approximated as a mixing approximation, giving the signals $f_c + f_m$ and $f_c - f_m$. This approximation would be used in Section 3.2 to explain the self-modulation property of the tunnel diode oscillators.

Bandwidth of FM signal. A frequency modulated signal is periodic in time t only when f_c is an integral multiple of f_m. Otherwise, the bandwidth is infinite with multiple sidebands in the frequency spectrum and each sidebands' strength can be estimated using a different version of the Eq. 7 using Bessel functions [31]. Using Carson's formula we can approximate the bandwidth containing the most of the signal power (99%) given by

$$BW \approx 2(\Delta f + f_m) = 2f_m(\beta + 1) \tag{10}$$

For non-sinusoidal signals, f_m is replaced by the maximum frequency in the message signal. For FM-broadcast, the allowed maximum frequency deviation is 75 kHz, and the maximum frequency is 56 kHz when broadcasting mono, stereo, and radio data service (RDS), giving an approximate bandwidth of 266 kHz.

Once the carrier signal has been generated–using a stabilized TDO as illustrated in Figure 11–the next step is to modulate this carrier with the desired information. Recent systems have used the SoM property of tunnel diodes [49, 84] to combine baseband and carrier signals, effectively using the TDO as both an oscillator and a mixer. In contrast, our goal is to generate broadcasts compatible with commodity FM-receivers, which requires frequency modulation of the carrier signal. To achieve this, we exploit the influence of the negative resistance of the TDO on its carrier frequency, which we call self-modulation.

Self-modulation of TDOs. We modulate the carrier signal generated by a TDO with an analog baseband signal. We bias the tunnel diodes in the negative resistance region (Figure 5(b)), where even a slight change in the bias voltage alters the negative resistance and, consequently, the oscillation frequency. For example, consider a simplified lumped-circuit model that combines a tunnel diode with an LC resonant tank. In this model, we compute the oscillation frequency as [29]:

$$\omega_o = \sqrt{\frac{R_{nr} - R_T}{L_T C_j R_{nr}}} \tag{11}$$

This equation indicates that the carrier frequency is dependent on the negative resistance of the tunnel diode. Because the negative resistance depends on the bias voltage, we express the oscillation frequency as a function of the voltage signal, $\omega_o = f(v(t))$. When the voltage signal includes the message signal, $v(t) = v_{bias} + m(t)$, we approximate the oscillation frequency as $\omega_o \approx \omega_c + f(m(t))$, where ω_c represents the unmodulated carrier frequency and $f(m(t))$ captures the frequency deviation introduced by the message. Relating it to the Eq. 6, this corresponds to the $2\pi k_f \int_0^t m(\tau)$ term of the frequency modulated signal and explains the self-modulation property. In effect, the oscillator generates the carrier and performs FM modulation, eliminating the need for conventional FM modulation circuitry. We demonstrate this capability by feeding an audio signal into the TDO, and we show the resulting modulated signal captured by a spectrum analyzer in Figure 12(a).

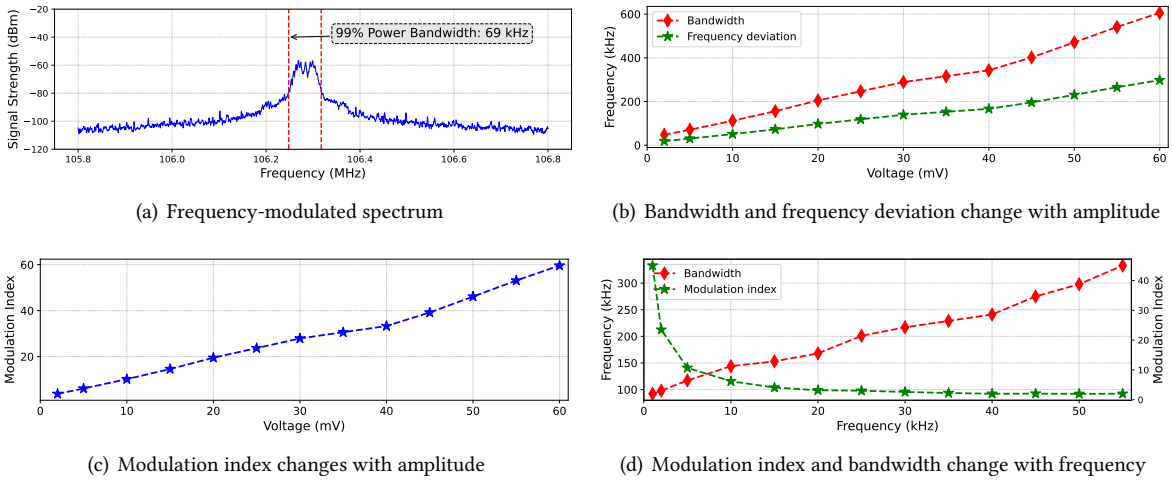

(a) Frequency-modulated spectrum

(b) Bandwidth and frequency deviation change with amplitude

(c) Modulation index changes with amplitude

(d) Modulation index and bandwidth change with frequency

Fig. 12. To understand self-modulation, we use a baseband signal composed of an audio tone with varying amplitude and frequency. Increasing the amplitude of the message signal raises the modulation index. Conversely, increasing the message frequency lowers the modulation index, causing the self-modulation behavior to transition into self-oscillating mixing. In this regime, the baseband signal mixes with the carrier rather than producing frequency modulation.

Understanding bandwidth, modulation index and baseband characteristics. We estimate the spectrum bandwidth in Figure 12(a) considering the occupancy of 99% power occupancy and applying Carson's formula (Eq. 10). Next, we calculate the maximum frequency deviation (Δf) and modulation index (β) for a message signal of known frequency and peak amplitude. We evaluated the impact of the message signal's amplitude on the frequency deviation. We provide a 5 kHz audio tone as the baseband signal to the transmitter. We vary the amplitude of the signal from 2 mV to 60 mV. We recorded the spectrum using a spectrum analyzer positioned at a distance of 1 m from the setup. Figures 12(b) and 12(c) show the result of the experiment. For each configuration, we estimate the bandwidth and frequency deviation ($\Delta f \approx \frac{BW}{2} - f_m$). We observe that Δf increases with the amplitude of the message signal and, consequently, the modulation index ($\beta = \frac{\Delta f}{f_m}$) also increases correspondingly. The frequency deviation also gives insights into the modulation sensitivity as $\Delta f = k_f A_m$.

Next, we vary the frequency of the message from 2 kHz to 60 kHz while maintaining a constant amplitude of 10 mV. With the amplitude fixed, the frequency deviation remains constant ($\Delta f = k_f A_m$ from Eq. 7). Therefore, the bandwidth increases linearly with frequency according to ($BW \approx 2(\Delta f + f_m)$). In contrast, the modulation index $\beta = \frac{\Delta f}{f_m}$ decreases inversely with the frequency of the message. This inverse relationship is pronounced at lower frequencies, as Figure 12(d) shows, which is consistent with theoretical expectations [31].

When the frequency of the message signal increases, the modulation index becomes very small ($\beta \ll 1$). At such low modulation indices, the resultant signal appears as a mixed signal, as explained in Section 3.2. This transition leads to the *self-oscillating mixing* property of the tunnel diode oscillators [84]. To evaluate the transition from modulation to mixing, we sweep the message signal frequency from 10 to 400 kHz while keeping the amplitude constant at 10 mV. We provide a detailed demonstration in our video[2]. At higher frequencies, the modulation becomes narrowband, and only the first sidebands appear prominently, leading to a SoM effect.

Modulating information as audio broadcasts. We demonstrated that the TDO can be frequency modulated using analog baseband signals and received through commodity FM-receivers. The natural question that follows is: *How can information be transmitted over such audio broadcasts ?* To address this, we draw inspiration from

[2] https://github.com/weiserlab/AudioCast/tree/main?tab=readme-ov-file#fm-modulation-vs-mixing

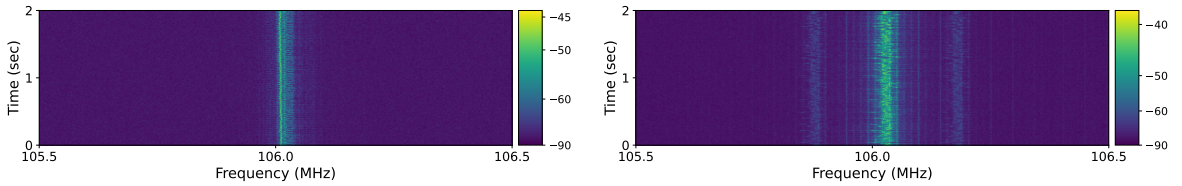

(a) Unmodulated carrier

(b) Simultaneous frequency modulation with analog signal together mixing with a digital baseband signal leveraging mixing property

Fig. 13. AudioCast supports frequency modulation with an analog audio signal while also exhibiting self-oscillating mixing property, enabling the simultaneous mixing of a complex baseband signal containing digital information.

data-over-sound techniques. We implement a Frequency-Shift Keying (FSK) modulation scheme, encoding data as distinct audio tones. We split the data into n-bit chunks and apply Reed-Solomon coding for error correction. We transmit T distinct, equally spaced tones in each transmission instance, transmitting $n \times T$ data bits per instance. We select these tones from a predefined spectrum within the audible range using the following equation:

$$F_i = f_0 + (i * 2^n + (data)_{10}) \cdot \Delta f \tag{12}$$

Where F_i is the frequency of the tone to be transmitted for the ith data chunk, f_0 is the starting frequency, n is the length of each data chunk, Δf is the frequency deviation between each tone and $(data)_{10}$ are the data of the chunk considered in its decimal (base10) representation. The transmitted message signal is thus the summation of the tones for each chunk, represented in the frequency domain by $m(f) = \sum_{i=0}^{T-1} F_i$ give the audio frame to be transmitted. Each audio frame is transmitted for a defined duration.

For example, in our experiments for evaluation in Section 4, a 1-byte data payload split into two 4-bit chunks, requiring $T = 2$ tones. Each data chunk can take on 16 (2^4) values, requiring 32 distinct frequencies that represent each value. We used a 1024-point FFT and a 48 kHz sampling rate (sample rate of general audio systems) at the receiver. To match, we select $\Delta f = \frac{48000}{1024} = 46.875$ Hz corresponding to one bin. Skipping the first 24 frequency bins results in a starting frequency of $f_0 = 1.125$ kHz. For frequency resolution, at least 1024 samples are required at 48 kHz, setting a minimum transmission time per payload to $t = \frac{1024}{48000} = 21.3$ms.

If we wish to transmit $i = 0$ data chunk with data $(0101)_2 = (5)_{10}$, the corresponding tone is $F_0 = f_0 + [0 * 2^4 + 5]\Delta f = 1359.375$Hz. The tones for the remaining values of i are computed similarly, generating the audio frame. The above implementation of the protocol yields a bit rate of approximately 46 bytes/sec (368 bps) using a 1.5 kHz span, ranging from 1.125 kHz to 2.625 kHz. The bitrate can be further improved by increasing the payload length, increasing the number of tones needed to cover the entire audio range. Using mono-audio allows for 15 kHz, while stereo-audio increases this to 45 kHz (15 + 30 kHz). This expansion enables transmission of up to 30 times more tones, potentially achieving a transmission bitrate of approximately 10.7 kbps. Additionally, if the receiver supports a more complex FFT (for example, 2048 point), we can further reduce Δf and lower the transmission time for each payload, further increasing the possible bitrate further.

Multiple streams for higher datarate. This work focuses on the encoding of audio and data as audio tones using the self-modulation property of tunnel diodes. However, we also recognize scenarios where the transmitter must support higher data rates, particularly for custom transceivers or software-defined radios. Furthermore, recent advances in digital radio broadcasting—such as HD Radio [1]—require higher data throughput and digital audio transmission. HD Radio, for example, uses an in-band on-channel (IBOC) system with orthogonal frequency division multiplexing (OFDM) subcarriers around the analog FM channel to deliver digital audio and data. In exploring this space, we discovered an additional property of the TDO: it can support simultaneous modulation and mixing of multiple baseband signals. This enables concurrent communication and audio broadcasting.

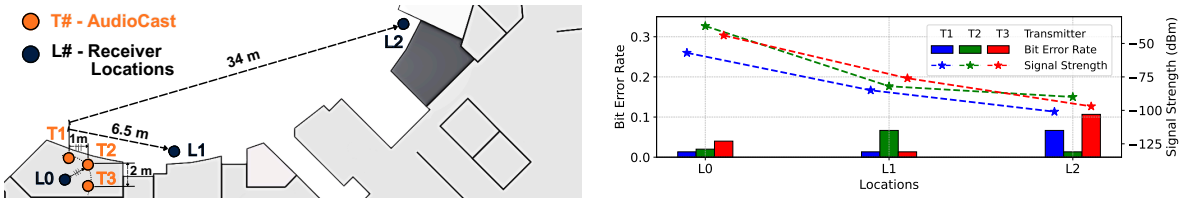

(a) Complex indoor environment with 3 AudioCast transmitters

(b) Bit error rate

Fig. 14. In a complex indoor environment with multiple AudioCast transmitters placed close to each other to transmit data simultaneously, the system performs reliably, demonstrating robustness to cross-interference. Three transmitters (T1, T2, and T3) are placed 1 m from each other and successfully transmit data over 34 m while maintaining a bit error rate (BER) < 0.11.

We evaluated this capability by feeding both an audio signal and a 150 kHz sine wave–representing an OFDM subcarrier–into the AudioCast transmitter. As shown in Figure 13(b), the resulting waterfall plot clearly displays both signals concurrently. Figure 13(a) shows the unmodulated carrier at 106.1 MHz, while the modulated carrier exhibits frequency modulation from the audio signal and sidebands at 105.95 MHz and 106.25 MHz due to the mixed sine wave. This multi-stream modulation opens up opportunities for more versatile communication, enabling the BB-transmitter to broadcast audio for standard FM-receivers while simultaneously transmitting higher-rate data for advanced receivers, such as those supporting HD Radio.

3.3 Reception

The receiver applies a 1024-point FFT with a sampling rate of 48 kHz on the recorded audio frames. To correctly decode the data, the receiver must know the payload length of the data (1 byte) transmitted in each audio frame. The Fourier transform is applied to the captured audio to obtain the frequency spectrum, which enables the receiver to decode binary data according to the pre-established encoding scheme. Finally, Reed-Solomon decoding is applied to the binary data to recover the original sensor information, providing an error correction step that mitigates potential transmission errors and ensures the integrity of the received data.

3.4 Supporting Multiple AudioCast Tags

AudioCast broadcasts can be received by commodity FM-receivers and chipsets such as the Si4703 [3]. Once demodulated, the audio or data can be further processed depending on the application. When data is transmitted, the decoding process begins as soon as the demodulated audio becomes available. To identify the beginning and end of a data transmission, we use specially crafted audio markers. These start and end markers provide a lightweight and computationally efficient mechanism for detecting encoded messages. During continuous recording of audio samples, the receiver searches for the presence of these markers and records all audio data between them for subsequent decoding. The start marker consists of a set of 16 specific frequencies transmitted in a single audio frame. We use the tones $f_0, f_0 + 3\Delta f, f_0 + 4\Delta f, f_0 + 7\Delta f, f_0 + 8\Delta f, \ldots, f_0 + 31\Delta f$ as the start marker, while the remaining 16 tones are used as the end marker.

AudioCast leverages frequency-division multiple access (FDMA) to support concurrent transmissions. Divides the FM-broadcast spectrum (88-108 MHz) into distinct channels, assigning to each transmitter a unique frequency. The adjacent channel selectivity of commodity FM-receivers—such as the Si4703—typically provides 50 dB suppression at ±200 kHz offsets [3], allowing the receiver to isolate the desired signal while rejecting interference from neighboring channels. With a 200 kHz spacing, multiple AudioCast transmitters can coexist without out-of-band interference, enabling dense and scalable deployments.

Although AudioCast is designed to enable reception using commodity FM-receivers, they can only demodulate one transmission at a time, necessitating dedicated receivers per transmitter or sequential re-tuning–introducing

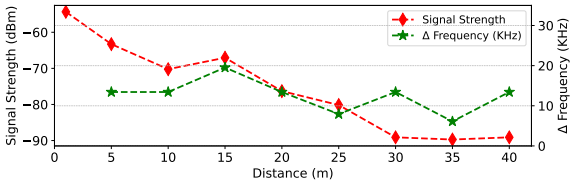

Fig. 15. Even in a complex indoor environment flanked by metallic objects in the roof and wall, the drift in the frequency of the signal generated by AudioCast transmitter remains small with a good SNR even at a distance (> 40m).

latency and complexity. To overcome this, AudioCast can also employ low-cost SDRs (e.g., RTL-SDR v4 [66]) as gateways. These SDRs support parallel demodulation of multiple signals within their 2.56 MHz bandwidth, allowing simultaneous reception of up to 10 AudioCast transmitters in a 2 MHz range. For larger deployments, advanced techniques like frequency-hopping, FTDMA, or dynamic spectrum access [12] can further optimize spectral efficiency and scalability. Furthermore, we can utilize medium access control techniques based on the Aloha protocol for each channel to support tens to hundreds of AudioCast tags transmitting concurrently.

Evaluation. We evaluated the impact of multiple AudioCast transmitters operating in close spectral and spatial proximity. In our experiment, three transmitters (T1, T2, T3) are placed 1 m apart in a university workspace, transmitting data simultaneously. We evaluated reception at three different locations (L0, L1, L2) in a nonlinear field of sight setup, as illustrated in Figure 14(a). The transmitters operate within a 1 MHz frequency span in the FM-broadcast band. We use a spectrum analyzer to measure the strength of the signal and take advantage of its FM demodulation capability to decode transmissions. Alternatively, a low-cost SDR-based receiver, as discussed earlier, can be used for reception. To assess link performance, we collect 150 fixed-length packets per iteration and repeat the process across multiple trials at each receiver location. We calculate PRR and BER at each receiver location, reporting only the BER in Figure 14(b) for brevity. The results demonstrate that even with closely spaced transmitters, each device operates independently and remains robust against self-interference.

4 Evaluation

We evaluated AudioCast under various environments and conditions. Our main findings are as follows.

- AudioCast transmits data over distances of up to 130 m in an outdoor LoS environment while consuming less than 200 µW of power without requiring the carrier emitter device in the embedded deployment.
- AudioCast operates reliably in multipath-rich environments, such as challenging indoor or urban settings, and supports communication ranges of several tens of meters. Additionally, it maintains an audio quality that is both perceptible and intelligible to users, with PESQ scores exceeding 1.29.

Setup. We experimented in different scenarios. For the line-of-sight (LoS) scenario, we conducted the experiments in outdoor and indoor environments flanked by walls, metallic objects on the roof, and in an open outdoor field, as shown in Figure 1, Figure 18(a) and Figure 19(a). The enclosed area exhibits complex propagation characteristics, characterized by reflections and multipath losses. The outdoor open field environment enables us to establish a baseline for the maximum communication range achievable by our system. We also experimented in a non–line–of–sight (NLoS) environment, which is an indoor office space (see Figure 16(a)) with multiple walls between the transmitter and receiver. This setup represents a realistic environment for embedded deployments.

We configured AudioCast to operate within the FM-broadcast band (see Figure 11), ensuring compliance with the allowed FM frequencies at our experimental locations (Singapore). In controlled experiments, we introduced the modulating signal as an audio or digital baseband waveform using a signal generator (Analog Discovery 3 [17], shown in Figure 8). For all other scenarios, we relied on our custom hardware platform. To capture the spectrum, we used a SignalHound BB60C spectrum analyzer [33]. For audio demodulation and reception, we use the Si4703

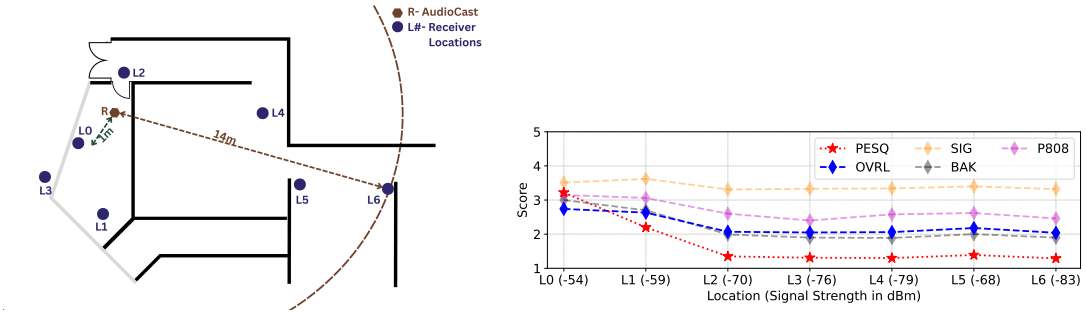

(a) Indoor NLoS environment (b) AudioCast speech quality scores

Fig. 16. We capture signal strength and broadcasted audio at different locations. We estimate the audio quality using PESQ and DNSMOS-based metrics. At location L6, farthest in our environment, we observe a PESQ = 1.29 and quality OVRL = 2.04, which is still sufficient for supporting applications involving processing through an ASR, or are human understandable.

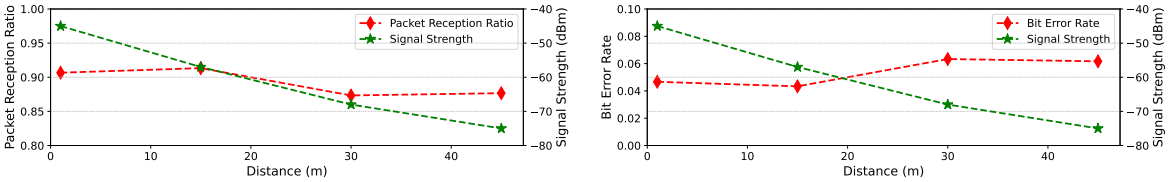

(a) Packet reception ratio (b) Bit error rate

Fig. 17. Even in complex indoor environments—with metallic surfaces, walls, and other obstructions—the AudioCast transmitter achieves communication ranges exceeding 45 m while maintaining high link reliability (BER = 0.069). This is sufficient to enable wide range of indoor sensing applications, including actuation and smart home deployments.

FM tuner chip [3], with decoded audio data processed via a microcontroller (Espressif ESP32-C3-Devkit). We also verified the successful reception of AudioCast transmissions using commodity FM-radio receivers.

Unmodulated transmitter stability. We evaluated the frequency drift of an unmodulated AudioCast transmitter in an indoor LoS environment characterized by walls and significant multipath effects. In the experiment, the location of the AudioCast transmitter was kept fixed while the position of the spectrum analyzer was varied to record the signal strength and frequency drift. Figure 15 presents the results, showing that despite the complex propagation conditions, the frequency drift of the carrier signal remains minimal (< 30 kHz). This experiment demonstrates the improved stability achieved through the design enhancements incorporated into the BB-transmitter architecture.

Audio quality. We evaluate the audio quality of AudioCast broadcasts in a NLoS setup, as shown in Figure 16(a). We supply a 30-second speech snippet as the baseband to the transmitter. The transmitter is located at location R, and the received audio is recorded at seven different receiver locations, labelled L0 through L6. To quantify audio quality, we compute the Perceptual Evaluation of Speech Quality (PESQ) metric [65], following the ITU-T P.862 standard. PESQ yields scores ranging from -0.5 to 4.5, with 4.5 indicating excellent quality. Although PESQ correlates with the Mean Opinion Score (MOS), it remains an objective metric rather than a direct measurement of MOS. For our analysis, we resample the audio snippets to 8 kHz and employ a full-reference method under narrowband conditions to compute the PESQ values [46]. This setup is appropriate since the typical voice frequency range spans 300 to 3.4 kHz [28], and PESQ was developed to evaluate narrowband audio. In addition to PESQ, we also use the DNSMOS P.835 metric [63], which provides improved correlation with MOS values. We implement DNSMOS using Speechmos [73] and obtain four key metrics to assess the degradation of audio

(a) Complex outdoor LoS environment

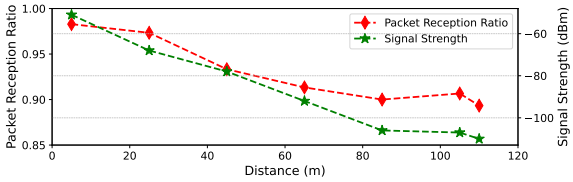

(b) Packet reception ratio

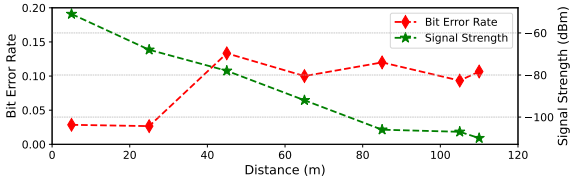

(c) Bit error rate

Fig. 18. Even in the presence of ambient FM-broadcasts and when AudioCast signal propagates through complex environments—including buildings and vegetation—AudioCast maintains high link quality. AudioCast successfully transmits data over distances up to 110 meters, achieving a received strength of -109 dBm, a PRR of 0.89, and a BER of 0.1067. These metrics are sufficient to support a variety of outdoor applications, such as networking sensors in farms or cities.

quality: Speech Quality (SIG), Background Noise Quality (BAK), Overall Audio Quality (OVRL), and the ITU-T P.808 Score (P808). DNSMOS scores range from 1 to 5, with 5 indicating excellent quality.

In the experiment, we measured the signal strength of AudioCast transmission received at each location using a spectrum analyzer to assess the relationship between signal quality and captured audio. The PESQ and DNSMOS results for the seven receiver locations are shown in Figure 16(b). We used a standard scale for both, as our measured PESQ and DNSMOS metrics did not go below 1. Although PESQ scores below one generally indicate poor intelligibility, the threshold for acceptable quality depends on the application. In constrained environments, scores around one can still enable basic speech recognition (ASR), whereas higher scores ($\geq$ 3) are generally required for high-quality communication. We also empirically verified that advanced ASR systems can achieve a word error rate (WER) of < 10% under these conditions, as demonstrated in Section 5.1. We also provide audio clips of the transmitted and received speech, together with the calculated PESQ values, in a video[3].

Link quality. We evaluated the link quality of AudioCast transmissions communicated via distinct audio tones. The experiments were carried out in three environments: indoor, semi-outdoor, and outdoor. The transmitter received a baseband audio signal that carried encoded data, as described in Section 3.2. To assess link quality, we transmitted a fixed-length packet 300 times, repeating the process over multiple iterations. We captured the received data using an Si4703 receiver interfaced with an ESP32 microcontroller and analyzed the spectrum using a Signal Hound BB60C spectrum analyzer. Figures 17(a) and 17(b) present the link quality metrics at various distances for the indoor scenario shown in Figure 1, which represents a challenging indoor environment. Although signal strength declines with distance, we observe a high packet reception ratio (PRR) of 0.87 and a reasonably low bit error rate (BER) of 0.069. Due to space constraints, our maximum evaluation distance was limited to 45 meters. However, the high SNR measured at that distance, well above the receiver noise floor, suggests the potential for achieving an even greater range.

We further evaluated AudioCast in a complex, semi-outdoor environment characterized by clear LoS but surrounded by buildings. In this setup, the transmitter was placed in the basement of a university building, facing an open road that extended outside, as shown in Figure 18(a). This configuration created a unique scenario where

[3] https://github.com/weiserlab/AudioCast/tree/main?tab=readme-ov-file#indoor-nlos-audio-evaluation

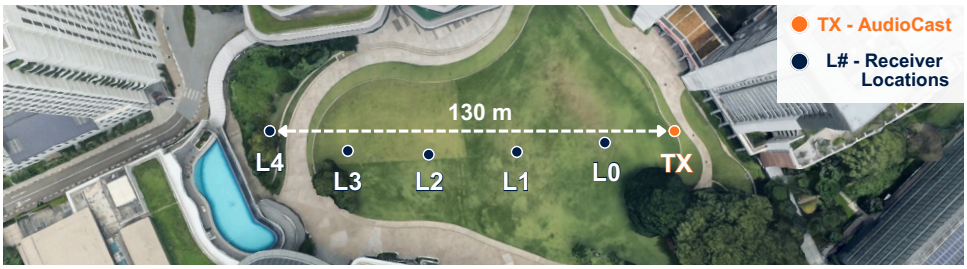

(a) Outdoor LoS environment

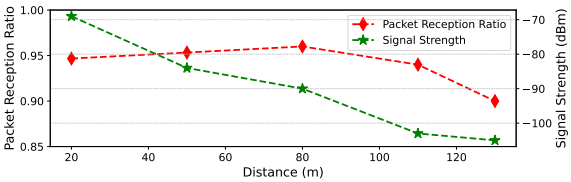

(b) Packet reception ratio

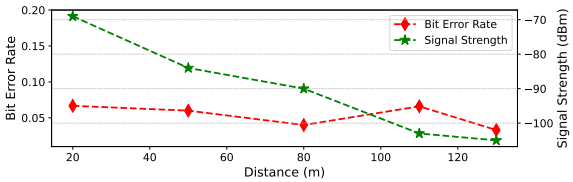

(c) Bit error rate

Fig. 19. In an outdoor environment, even with potential strong interference from ambient FM broadcasts, AudioCast maintains high link quality. In LOS conditions, the system successfully transmits data up to 130 m, achieving a received signal strength of -105 dBm, a packet reception ratio of PRR = 0.9, and a bit error rate of BER = 0.033.

the signal traversed both indoor and outdoor spaces, with the transition occurring approximately 40 m from the transmitter. In such environments, the system is more susceptible to interference from ambient FM broadcasts, particularly in outdoor settings. Figures 18(b) and 18(c) present the link quality metrics measured at various distances. We achieved a PRR of 0.89 and a BER of 0.1067 at a communication distance of 110 m. Importantly, no significant interference from ambient FM transmissions was observed during these tests.

Finally, we evaluate AudioCast in a fully outdoor environment, as shown in Figure 19(a). The transmitter and receiver are located in an open area with minimal obstructions (e.g., trees), allowing us to evaluate the performance of the system under ideal LoS conditions. The results, presented in Figures 19(b) and 19(c), highlight the system's ability to maintain high link quality over extended distances. AudioCast successfully transmits data up to 130 meters, achieving a received signal strength of -105 dBm, a PRR of 0.9 and a BER of 0.033. These results confirm the robustness of AudioCast in outdoor deployments, even in the presence of ambient interference.

We summarize the results of the experiment in Table 2. These results highlight the system's ability to support a large communication range, making it suitable for both indoor and outdoor embedded deployments, such as smart homes, soil monitoring sensors, or city-wide sensor networks that communicate with edge devices.

High bitrate transmissions. In this experiment, we evaluate AudioCast's ability to support scenarios that require the transmission of larger volumes of data at higher bitrates, which are then received using a custom receiver such as a software-defined radio. Specifically, we assess the system's capacity to mix higher-frequency baseband signals using on-off keying (OOK) modulation while varying the intermediate frequency from 100 kHz to 5 MHz. The baseband signal is generated using a function generator (Analog Discovery 3). The resulting mixed signals appear as side peaks around the carrier in the spectrum analyzer, as shown in Figure 20(a). We also track the strength of these sidebands with varying distances. Although the signal strength decreases with distance, it remains relatively stable throughout the evaluated frequency range (see Figure 20(b)). However, at higher baseband frequencies, a reduced modulation index further weakens the sidebands (as described in Equation 9). These findings suggest that AudioCast may support wideband baseband signals with more complex modulation

Table 2. Summary of AudioCast's performance across various environments.

Environment	Setup	Distance (m)	RSS (dBm)	PRR	BER	PESQ
Indoor	NLoS	14	-83	-	-	1.29
Indoor	LoS	45	-78	0.87	0.069	-
Complex-Outdoor	LoS	110	-109	0.89	0.1067	-
Outdoor	LoS	130	-105	0.9	0.033	-

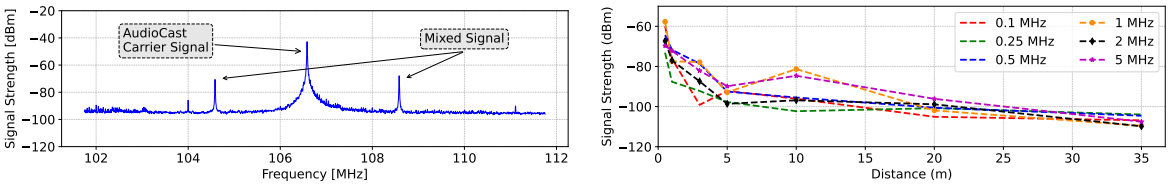

(a) Spectrum with 2 MHz mixed signal

(b) Signal strength for different baseband signal frequencies

Fig. 20. To preserve compatibility with commodity FM-receivers, AudioCast transmits information as audio broadcasts. However, this approach limits both reliability and bitrate. AudioCast can support higher bitrates by employing complex modulation schemes and wider bandwidth at the cost of reduced range and the need for more complex receiver designs.

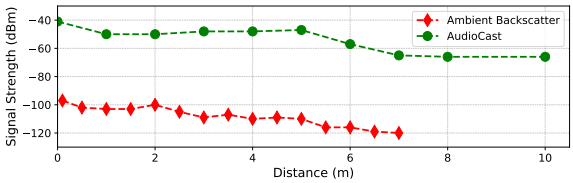

Fig. 21. Ambient FM-broadcasts are inherently weak, and when combined with the losses associated with the backscatter process, result in even weaker emissions and significantly limited range. In our experiments, the ambient backscatter tag achieved a range of only 7 m, compared to the 45 m range achieved by AudioCast under similar conditions.

schemes to achieve higher data rates. However, since the system focuses on compatibility with ubiquitous FM receivers, we leave the full exploration of higher-bitrate transmission for future work.

Comparison with ambient backscatter. We compare the received signal strength of the AudioCast with that of an ambient backscatter transmitter [88]. The backscatter system used the signal from the 89.3 MHz radio station, which had the highest signal strength at the test location (-70 dBm). The results, shown in Figure 21, highlight a limitation of the ambient backscattering mechanism: its received signal strength is significantly weaker than that of the AudioCast transmitter. The maximum range for the backscatter system was only 7 m, whereas the AudioCast's transmitter achieved a range exceeding 45 m. We observed a similar trend in other test locations. Thus, further highlighting the advantage of the BB-transmitter over ambient backscatter.

Power consumption. We evaluated the power of AudioCast using a baseband generator (Figure 7(e)) designed using the MSP430FR5959 microcontroller [36]. The microcontroller, operating at 1.9 V using the Nordic PPK2 Power Profiler Kit [69] in source meter mode, generated PWM signals with a duty cycle of 50 % in low-power modes. For frequencies up to 353 Hz, an internal low-frequency oscillator was used; for frequencies up to 500 kHz, the CPU frequency was set to 1 MHz. The total power consumption remained below 200 µW and varied with the baseband frequency used as shown in Table 3. The baseband signal was interfaced with the AudioCast transmitter using a resistor divider to reduce harmonic distortion and bandpass filters to eliminate harmonics. For evaluation, we generated monotone signals. Power consumption could be further reduced by ASIC instantiation.

Table 3. The AudioCast transmitter, including its baseband generator backend, consumes less than 200 µW of total power.

Baseband Frequency (Hz)	Baseband Generator Min. Power Consumption (µW)	Total Power Consumption (µW)
0 – 353	28	**82.73**
354 – 1.2k	61.24	**115.97**
1.2k – 500k	87.84	**142.57**
> 500k	145.62	**200.35**

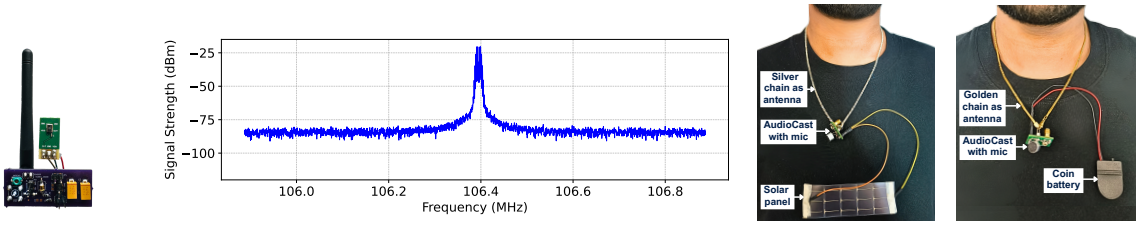

(a) Tracker prototype using AudioCast for low-power offloading of microphone signal

(b) Carrier modulated with microphone signal

(c) AudioCast using silver chain as antenna and powered through flexible solar-cell

(d) AudioCast using gold chain as antenna and powered through a coin cell

Fig. 22. AudioCast enables the realization of a tracker for monitoring vocal interactions. A microphone is coupled with the AudioCast transmitter, which directly modulates the carrier signal to produce a frequency-modulated signal. Commodity FM-radio receivers can then receive this signal. The FM-broadcast spectrum's lower wavelength and favourable propagation properties allow the use of chains or wires as antennas, enabling efficient signal transmission.

5 Use Cases

We prototype three application scenarios to demonstrate the real-world applicability of AudioCast.

5.1 Low-power Wireless Voice Tracker

The tracking of voice plays a vital role in our lives, allowing us to take notes by transcribing spoken words, monitor our daily activities, and even track our health [11, 16, 62, 90]. Mobile phones, smartwatches, and earphones are used to support these applications. However, they are battery-operated devices and face a key challenge: recording and streaming audio wirelessly consumes significant energy. Even basic audio tracking requires amplifiers and complex processing, further draining the battery. In addition, they must also overcome challenges such as distinguishing multiple speakers, determining the direction of speech, and operating robustly in noisy environments [16, 90]. Performing these complex processing further leads to a shorter battery life.

AudioCast can enable voice communication by implementing a low-power tracker. The tracker would sense the audio and transmit it with minimal processing, while the edge device handles computationally intensive tasks [76]. The tracker is enabled due to the low-power nature of AudioCast and the self-modulation property. A microphone without an amplifier can modulate the carrier signal with audio and transmit it over an FM-broadcast band. These characteristics enable continuous operation for days on a coin cell battery or even on harvested energy, as demonstrated in Figure 22. In fact, using a CR2032 coin cell with a capacity of 235 mAh and a voltage of 3 V, we estimate that it can support the tracker's continuous operation for 146 days.

We envision AudioCast trackers integrated into wearable garments, leveraging advances in FM antenna design [88], or worn as pendants where the necklace chain or cable serves as an antenna. This is feasible because of the longer wavelengths and favorable propagation characteristics of the FM-broadcast spectrum, which reduce signal losses from proximity to the human body and enable long-range communication. In Figures 22(c) and 22(d), we evaluate the AudioCast transmitter using a silver chain and a gold chain as the transmission antenna.

Due to its lower resistivity, the silver chain ($\rho = 15.9\,n\Omega\,m$) provides better radiated power compared to gold ($\rho = 22.4\,n\Omega\,m$). We measured the signal strength using a spectrum analyzer placed 1 m away from the user wearing the transmitter. The signal strength for the silver chain was found to be −38 dBm, while the gold chain a signal strength of −42 dBm, which is sufficiently strong for reception using commodity FM-receivers.

An edge device can receive AudioCast transmissions for further processing, such as performing transcription. We prototype a device to demonstrate this scenario. As shown in Figure 22(a), our transmitter is directly coupled with a MEMS microphone (AMM-3742-T, PUI Audio) [8]. A speaker placed 30 cm away, a typical distance for a pendant microphone from a user's mouth, generates a 5 kHz audio signal. The microphone signal directly modulates the carrier frequency, taking advantage of the self-modulation property of the tunnel diode oscillator, as illustrated in Figure 22(b). Next, we evaluate the performance of transmitted and received audio for automatic speech recognition (ASR). Using Whisper [57], we measure the word error rate (WER) of the transcribed text against the ground truth. Even without de-noising, the WER remains low (Figure 23).

Scenarios. We envision numerous scenarios that the tracker can enable. In assisted living facilities, AudioCast can serve as a low-power voice interface for health monitoring. Residents can wear microphones equipped with AudioCast trackers to record health updates and dictate notes. Another scenario involves individuals using tracker to record and track conversations, which can then be transcribed later on an edge device.

Audio backscatter. The tracker builds on recent efforts to offload audio via the backscatter mechanism, but prior work faces significant limitations. Talla et al. present a CRFID-based tag with a microphone, which achieves only a few meters of range using RFID readers [77]. They also describe a battery-free smartphone that uses backscatter, where the microphone interfaces directly with the backscatter module; however, strong self-interference limits reception to short ranges and requires SDR receivers [76]. Similarly, Zhao et al. use analog backscatter to transmit audio from a microphone array over distances up to 28 m, but again rely on SDRs [96]. Ekhonet et al. connect microphones directly to backscatter modules, removing the need for local processing, but their system remains restricted to a few meters [94]. All of these systems are dependent on complex power-hungry SDRs or RFID readers for reception. In contrast, AudioCast supports significantly longer ranges and leverages ubiquitous low-cost FM receivers (e.g. smartphones, car radios) for reception. Moreover, unlike backscatter systems, AudioCast eliminates the need for a carrier emitter device or strong ambient signals, simplifying real-world deployment.

5.2 Interacting with Computing Devices and Appliances

The ability to communicate gestures wirelessly has numerous applications, including interaction with computing devices [39, 44]. However, current wireless gesture sensors rely on complex and power-hungry components that track signals and communicate over short distances using energy-intensive transceivers. AudioCast's characteristics offer the potential to simplify this design, enabling low-power wireless gesture recognition that can be used to control actuators or computing devices, which then perform the corresponding actions. We prototype a gesture recognition system based on previous work showing that hand gestures induce distinctive variations in light intensity [42, 43, 82, 86]. We connect a photoresistor sensor to AudioCast and transmit light variations via frequency-modulated signals to an FM-receiver.

The experiment was carried out in an indoor university setting under ambient lighting. The sensor output was used directly as the biasing voltage for the AudioCast transmitter (Figure 24(a)). Since both the transmitter bias and the sensor output voltage are in the millivolt range, no additional amplification was needed. The transmitter was tuned to 106.5 MHz and placed on a table. A user performed two hand gestures near the sensor: a single tap and three consecutive taps. A spectrum analyzer placed 1 m away captured the transmitted signal; however, given the range of AudioCast, the receiver could be placed tens of meters away. The sensor output fluctuated between 10 and 20 mV during gestures, altering the bias of the tunnel diode and shifting the resonant frequency.

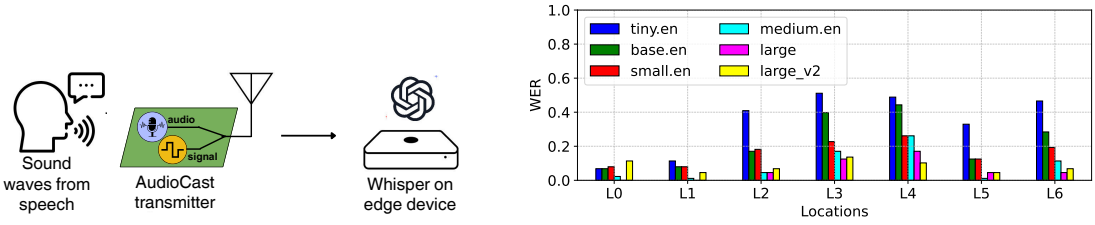

(a) AudioCast as a low-power vocal interface

(b) Word error rate (WER) of transcribed audio received from the AudioCast transmitter

Fig. 23. AudioCast can be used as a low-power vocal interface to connect with the edge devices that can do automatic speech recognition (ASR). The system can be used for applications like transcription of meetings, or lifelogging.

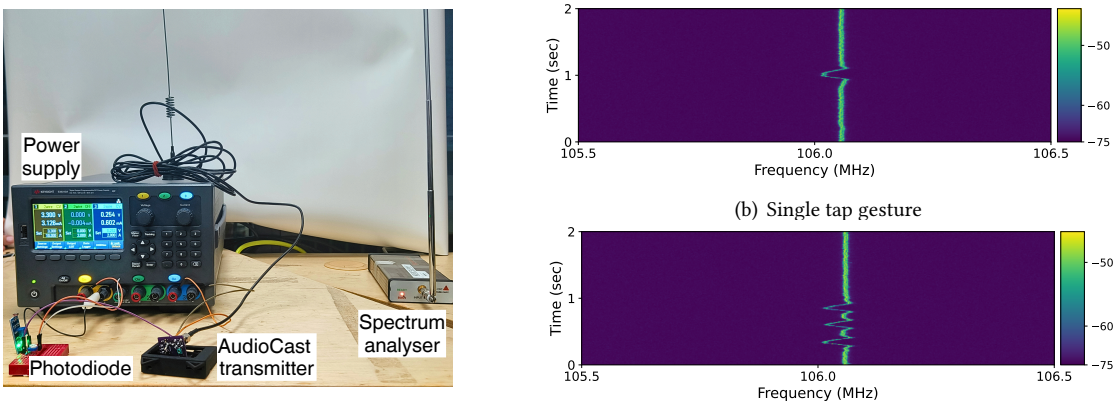

(a) Experimental setup

(b) Single tap gesture

(c) Triple tap gesture

Fig. 24. AudioCast enables the design of low-power wireless gesture sensors. We prototype a light-based gesture sensor that detects hand gestures (e.g., single-tap or triple-tap) via changes in light intensity. The sensor transmits these gestures using AudioCast, which are then classified at the edge device to trigger actions (e.g., controlling appliances).

These shifts, visualized in the waterfall graphs in Figures 24(b) and 24(c), demonstrate the ability of AudioCast to capture gestures wirelessly. These frequency patterns can be analyzed using machine learning techniques.

Backscatter sensors. Our work builds on the gesture sensing system introduced by Varshney et al. [82], which senses hand gestures using a solar cell and communicates using the backscatter mechanism. In contrast, our system achieves a significantly greater range, eliminates the need for a carrier emitter because of the BB-transmitter architecture, and leverages an off-the-shelf FM-broadcast receivers for reception, making it a more practical solution. The simplicity of our design can enable for a wide range of applications. For example, a user can control home devices, such as an air conditioner or television, using simple gestures. Due to its low power consumption, an AudioCast equipped sensor could last for years without requiring battery replacement.

5.3 Backhauling using Ubiquitous FM-broadcast Receivers

The deployment of embedded systems in large and remote areas is increasing rapidly, supporting applications in agriculture [85], urban monitoring [4], and environmental sensing. In many of these deployments, the traditional communication infrastructure, such as cellular networks, is not available, preventing the direct transmission of the collected sensor data. This limitation has sparked growing interest in opportunistic networks that leverage

the ubiquity of computing devices, including mobile phones, smartwatches, and smart vehicles, as data mules to collect and relay information from these remote sensor deployments opportunistically.

Park et al. [54] explored the feasibility of using mobile phones as data mules for sensor networks. Commercial systems such as Apple's Find My and Amazon's Sidewalk now offer widespread coverage. Recent research has shown that sensor nodes can operate similarly to AirTags, transferring sensor data through Apple's infrastructure [10, 32]. Likewise, Amazon's Sidewalk [6] enables sensor devices to take advantage of existing smart home platforms to collect information and extend network connectivity opportunistically.

Given its long range and low-power operation, we envision that AudioCast is well-suited for outdoor applications. As demonstrated in our experiments, AudioCast supports communication over distances of up to 100 meters, which is sufficient to transmit sensor data. These favorable characteristics, combined with the ubiquitous availability of FM-broadcast receivers, can enable a new class of devices to function as data mules, collecting sensor data from deployments in farms, cities, and other large-scale environments.

We prototyped a system inspired by TagAlong [10], integrating AudioCast with Apple's Find My network. Specifically, we designed a setup in which AudioCast transmissions are received and relayed through the Find My network. To evaluate this approach, we performed two experiments. The first took place in an isolated location, with only one Apple device receiving BLE advertisements. The second was in an office environment with approximately 30–40 nearby Apple devices. The results are shown in Figure 25. Our evaluation focused on two key metrics: the latency between data transmission and reception using Datafetcher, and the reliability of packet delivery. As expected, latency decreased with a higher density of Apple devices, with the office environment achieving a median latency of 3 min (Figure 25(a)). The reliability of packet reception was strongly influenced by the broadcast interval, that is, how frequently packets were transmitted. Aligning the broadcast interval with the scanning frequency of Apple devices significantly improved packet pick-up. As shown in Figure 25(b), a broadcast interval of 0.3 seconds achieved nearly 99% packet delivery reliability. These results demonstrate that AudioCast can be effectively integrated into opportunistic networks such as Apple's Find My.

Scenario. We envision scenarios where sensors deployed in farms capture critical information about soil conditions. These sensors transmit data using the AudioCast transmitter over distances ranging from tens to hundreds of meters. FM-broadcasts from these sensors can be opportunistically received by cars, trucks, and other vehicles acting as data mules, which then offload the information to a central server for processing. Another application could involve an urban environment and build on the Signpost [4] platform, using the FM-broadcast spectrum to opportunistically offload citywide sensor data.

6 Discussion

Tunnel diode availability. Tunnel diodes are essential for the design of AudioCast. However, they are now commercially obsolete, making their procurement a significant challenge. Despite this, tunnel diodes have seen renewed interest due to their ability to enable low-power sensing [49, 78] and communication [5, 21, 80, 83, 84]. We hope that recent encouraging works [5, 18, 21, 49, 64, 80, 83, 84], including those of AudioCast, will motivate commercial interest and the large-scale fabrication of tunnel diodes in the future.

Unidirectional communication. Most communication in embedded systems involves collecting sensor data from the deployment and transmitting it to the broader computing infrastructure. Although AudioCast enables this functionality and is sufficient for retrieving data from embedded deployed systems, it does not currently support communication in the reverse direction, i.e., from the infrastructure to the system, if actuation or control is required. We plan to explore the potential for enabling bidirectional communication in AudioCast as part of our future work. In particular, we will build on our recent work, SoMix [47].

Low-bandwidth and bitrate. AudioCast focuses on low-bandwidth communication, making it well-suited for applications such as transmitting sensor data, audio, or simple commands. This design choice is driven by the goal

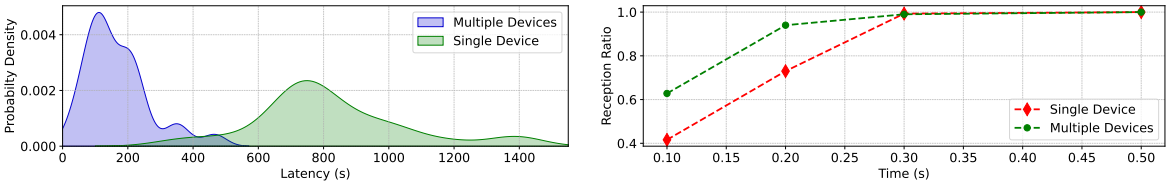

(a) End-to-end latency

(b) Data reception ratio with increasing broadcast time

Fig. 25. The time to retrieve a packet from Apple's servers decreases as the number of nearby Apple devices increases. The reception ratio improves with longer advertising durations, which increase the number of broadcasts per packet.

Table 4. AudioCast achieves low-power consumption than commercial transmitters while achieving comparable communication range. AudioCast supports most common embedded applications that require low bitrate communication.

Radio Technology	Frequency (MHz)	Data Rate (bps)	Energy Consumption (mW)	Estimated Range (m)
BLE (nRF52840) [68]	2400	125k, 500k, 1M, 2M	11.5 / 14.4 / 49.2	345
ZigBee (nRF52840)	2400	250k	19.2	280
SigFox (ATA8520E) [7]	868 – 870 / 902 – 906	100	95.4	10k
LoRa (SX1276) [71]	137 – 1020	293, 3.125k, 9.375k	66.0 / 95.7 / 287.1 / 396.0	4k – 6k
FM (Si4713) [72]	76 – 108	<= 1.4M (Audio)	60.39	10 – 20 (NLoS) 100 – 300 (LoS)
AudioCast	**88 – 108**	**368 – 10.7k** (Audio)	**0.2**	**> 14 (NLoS)** **130 (LoS)**

of compatibility with commodity FM-receivers, which are designed to receive audio broadcasts and inherently limit the achievable bitrate. However, if we relax this compatibility requirement, the system can be extended to support higher data rates, enabling applications that require greater bandwidth, such as real-time streaming video or large data transfers. Techniques like OFDM offer the potential for increased throughput, but come with added computational complexity, such as FFT calculations, that significantly increase power consumption. Furthermore, aggregating unused channels in the FM spectrum could provide wider bandwidths, supporting more simultaneous communication channels, and a overall higher bitrate.

Commercial transmitters. A variety of radio transmitters are used in embedded applications, which typically support standards such as BLE, ZigBee, LoRa, SigFox and FM radio. We compare AudioCast with these transmitters in Table 4, presenting parameters such as bitrate, energy consumption, and estimated range based on datasheet specifications. AudioCast 's power consumption is just 200 µW, which is several orders of magnitude lower than other transmitters. This enables it to operate on a small coin cell battery or even on harvested energy for a much longer time duration. Despite the low-power design AudioCast, it achieves a communication range upto 130 m in LoS–comparable to much higher-power transmitters. Thus, AudioCast offers a unique combination of energy efficiency and range relative to existing transmitters.

7 Conclusion

We presented AudioCast, a solution to the connectivity challenges faced by embedded systems. The core contribution lies in the conceptualization of the Beyond-Backscatter transmitter, which achieves low-power operation without requiring a carrier emitter device. Additionally, we demonstrate the self-modulation property of tunnel diode oscillators, enabling frequency modulation of the carrier signal without the need for external circuitry. This allows compatibility with ubiquitous FM receivers found in cars and smartphones and facilitates the use of underutilized portions of the FM-broadcast spectrum. Our results show that the system achieves communication ranges of up to 130 m in LoS environments and 14 m in NLoS environments, while consuming only 200 µW of power. We prototype several applications, including a low-power wireless voice tracker, a gesture

recognition system, and FM-based backhauling, demonstrating the promise of the system for enabling low-power sensing and communication, as well as sustainable embedded deployments. This work is released as open-source, with design files and other details available at the following repository: https://github.com/weiserlab/AudioCast

Acknowledgments

The authors thank the anonymous reviewers for their insightful comments. The authors acknowledge Yuvraj Singh Bhadauria and Manoj Gulati for their assistance and support during the early stages of this work. This research is fully supported by the Advanced Research and Technology Innovation Centre (ARTIC) at the National University of Singapore under Grant (Project Number: WDSS-RP1, WBS: A-8000976-00-00). In addition, some parts of this work are supported by a Tier 1 grant from Ministry of Education (A-8001661-00-00). It is also supported by a Startup Grant from ODPRT (A-8000277-00-00) and an unrestricted gift from Google through their Research Scholar Program (A-8002307-00-00-00), all of which are hosted at the National University of Singapore.

References

[1] [n. d.]. HD Radio™ FM Transmission System Specifications. https://nrscstandards.org/standards-and-guidelines/documents/archive/nrsc-5-c/1026sf.pdf. [Accessed: 2024-11-01].

[2] [n. d.]. Report ITU-R SM.2028-2. https://www.itu.int/dms_pub/itu-r/opb/rep/R-REP-SM.2028-2-2017-PDF-E.pdf. [Accessed: 2024-07-02].

[3] [n. d.]. Skyworks | — Si4703. https://www.skyworksinc.com/en/Products/Audio-and-Radio/Si4702-03-FM-Radio-Receivers/Si4703. [Accessed: 2024-07-02].

[4] Joshua Adkins, Branden Ghena, Neal Jackson, Pat Pannuto, Samuel Rohrer, Bradford Campbell, and Prabal Dutta. 2018. The signpost platform for city-scale sensing. In *Proceedings of the 17th ACM/IEEE International Conference on Information Processing in Sensor Networks* (Porto, Portugal) *(IPSN '18)*. IEEE Press, 188–199. https://doi.org/10.1109/IPSN.2018.00047

[5] Francesco Amato. 2017. *Achieving hundreds-meter ranges in low powered RFID systems with quantum tunneling tags.* Ph. D. Dissertation. Georgia Institute of Technology. http://hdl.handle.net/1853/58228

[6] Amazon.com. 2024. Everything you need to know about Amazon Sidewalk, the secure, low-cost network that can connect devices up to half a mile away. https://www.aboutamazon.com/news/devices/everything-you-need-to-know-about-amazon-sidewalk. [Online; Accessed: 2024-07-01].

[7] Atmel. 2025. Atmel 9409 Smart RF ATA8520E Datasheet. https://ww1.microchip.com/downloads/aemDocuments/documents/OTH/ProductDocuments/DataSheets/Atmel-9409-Smart-RF-ATA8520E_Datasheet.pdf. [Accessed: 2025-01-22].

[8] PUI Audio. n.d.. AMM-3742-2-T Datasheet. https://api.puiaudio.com/filename/AMM-3742-2-T.pdf [Accessed: 2025-01-25].

[9] Paramvir Bahl, Ranveer Chandra, Thomas Moscibroda, Rohan Murty, and Matt Welsh. 2009. White Space Networking with Wi-Fi like Connectivity. In *Proceedings of the ACM SIGCOMM 2009 Conference on Data Communication* (Barcelona, Spain) *(SIGCOMM '09)*. Association for Computing Machinery, New York, NY, USA, 27–38. https://doi.org/10.1145/1592568.1592573

[10] Alex Bellon, Alex Yen, and Pat Pannuto. 2023. TagAlong: Free, Wide-Area Data-Muling and Services. In *Proceedings of the 24th International Workshop on Mobile Computing Systems and Applications* (Newport Beach, California) *(HotMobile '23)*. Association for Computing Machinery, New York, NY, USA, 103–109. https://doi.org/10.1145/3572864.3580342

[11] Sarnab Bhattacharya, Rebecca Adaimi, and Edison Thomaz. 2022. Leveraging Sound and Wrist Motion to Detect Activities of Daily Living with Commodity Smartwatches. *Proc. ACM Interact. Mob. Wearable Ubiquitous Technol.* 6, 2, Article 42 (July 2022), 28 pages. https://doi.org/10.1145/3534582

[12] Tusher Chakraborty, Heping Shi, Zerina Kapetanovic, Bodhi Priyantha, Deepak Vasisht, Binh Vu, Parag Pandit, Prasad Pillai, Yaswant Chabria, Andrew Nelson, Michael Daum, and Ranveer Chandra. 2022. Whisper: IoT in the TV White Space Spectrum. In *19th USENIX Symposium on Networked Systems Design and Implementation (NSDI 22)*. USENIX Association, Renton, WA, 401–418. https://www.usenix.org/conference/nsdi22/presentation/chakraborty

[13] Spyridon Nektarios Daskalakis, John Kimionis, Ana Collado, George Goussetis, Manos M. Tentzeris, and Apostolos Georgiadis. 2017. Ambient Backscatterers Using FM Broadcasting for Low Cost and Low Power Wireless Applications. *IEEE Transactions on Microwave Theory and Techniques* 65, 12 (2017), 5251–5262. https://doi.org/10.1109/TMTT.2017.2765635

[14] Spyridon-Nektarios Daskalakis, John Kimionis, Ana Collado, Manos M. Tentzeris, and Apostolos Georgiadis. 2017. Ambient FM backscattering for smart agricultural monitoring. In *2017 IEEE MTT-S International Microwave Symposium (IMS)*. 1339–1341. https://doi.org/10.1109/MWSYM.2017.8058860

[15] Jasper de Winkel, Vito Kortbeek, Josiah Hester, and Przemysław Pawełczak. 2020. Battery-Free Game Boy. *Proc. ACM Interact. Mob. Wearable Ubiquitous Technol.* 4, 3, Article 111 (Sept. 2020), 34 pages. https://doi.org/10.1145/3411839

[16] Artem Dementyev, Dimitri Kanevsky, Samuel Yang, Mathieu Parvaix, Chiong Lai, and Alex Olwal. 2023. LiveLocalizer: Augmenting Mobile Speech-to-Text with Microphone Arrays, Optimized Localization and Beamforming. In *Adjunct Proceedings of the 36th Annual ACM Symposium on User Interface Software and Technology* (San Francisco, CA, USA) *(UIST '23 Adjunct)*. Association for Computing Machinery, New York, NY, USA, Article 75, 3 pages. https://doi.org/10.1145/3586182.3615789

[17] Digilent. 2025. Analog Discovery 3: 125 MS/s USB Oscilloscope, Waveform Generator, Logic Analyzer, and Variable Power Supply. https://digilent.com/reference/test-and-measurement/analog-discovery-3/specifications?srsltid=AfmBOorkzfdqKTMuvdYxJ4LjMWAGNHavQ8X8GOfnQjb0Xe86zPWR9jTy. [Accessed: 2025-04-20].

[18] Huixin Dong, Yirong Xie, Xianan Zhang, Wei Wang, Xinyu Zhang, and Jianhua He. 2023. GPSMirror: Expanding Accurate GPS Positioning to Shadowed and Indoor Regions with Backscatter. In *Proceedings of the 29th Annual International Conference on Mobile Computing and Networking* (Madrid, Spain) *(MobiCom '23)*. Association for Computing Machinery, New York, NY, USA, Article 11, 15 pages. https://doi.org/10.1145/3570361.3592511

[19] DRS. [n. d.]. List of radio stations in New Delhi. https://onlineradiostations.in/delhi/. [Accessed: 2024-07-02].

[20] Prabal Dutta. 2011. Sustainable sensing for a smarter planet. *XRDS* 17, 4 (June 2011), 14–20. https://doi.org/10.1145/1961678.1961680

[21] Aline Eid, Jimmy Hester, and Manos M. Tentzeris. 2020. A 5.8 GHz Fully-Tunnel-Diodes-Based 20 µW, 88mV, and 48 dB-Gain Fully-Passive Backscattering RFID Tag. In *2020 IEEE/MTT-S International Microwave Symposium (IMS)*. 607–610. https://doi.org/10.1109/IMS30576.2020.9224116

[22] Electronic Code of Federal Regulations. [n. d.]. Title 47, Part 15 - Radio Frequency Devices. https://www.ecfr.gov/current/title-47/chapter-I/subchapter-A/part-15 [Accessed: 2024-10-29].

[23] Joshua F. Ensworth and Matthew S. Reynolds. 2017. BLE-Backscatter: Ultralow-Power IoT Nodes Compatible With Bluetooth 4.0 Low Energy (BLE) Smartphones and Tablets. *IEEE Transactions on Microwave Theory and Techniques* 65, 9 (2017), 3360–3368. https: //doi.org/10.1109/TMTT.2017.2687866

[24] Fandom. [n. d.]. List of radio stations in Stockholm, Sweden. https://russel.fandom.com/wiki/List_of_radio_stations_in_Stockholm,_Sweden. [Accessed: 2024-07-02].

[25] FCC. [n. d.]. List of radio stations in New York. http://www.fcc.gov/mb/audio/fmq.html. [Accessed: 2024-07-02].

[26] Federal Communications Commission. 2022. Unlicensed White Space Device Operations in the Television Bands: Second Order on Reconsideration and Order, ET Docket Nos. 04-186 and 14-165. https://docs.fcc.gov/public/attachments/DOC-400041A1.pdf [Accessed: 2024-10-29].

[27] Federal Communications Commission (FCC). 1993. Understanding the FCC Regulations for Low-Power, Non-Licensed Transmitters. https://transition.fcc.gov/oet/info/documents/bulletins/oet63/oet63rev.pdf. [Accessed: 2025-01-16].

[28] Roger L. Freeman. 2005. *Fundamentals of Telecommunications* (3rd ed.). Wiley-Interscience. https://www.pce-fet.com/common/library/books/51/9134_FundamentalsofTelecommunications_R.Freeman.pdf

[29] Sylvester P. Gentile. 1962. *Basic Theory and Application of Tunnel Diodes.* D Van Nostrand Company Inc.

[30] Jeremy Gummeson, Shane S. Clark, Kevin Fu, and Deepak Ganesan. 2010. On the limits of effective hybrid micro-energy harvesting on mobile CRFID sensors. In *Proceedings of the 8th International Conference on Mobile Systems, Applications, and Services* (San Francisco, California, USA) *(MobiSys '10)*. Association for Computing Machinery, New York, NY, USA, 195–208. https://doi.org/10.1145/1814433.1814454

[31] Simon Haykin. 2006. *The Introduction to Analog and Digital Communications 2nd Edition with Wiley Plus Set.* John Wiley & Sons, Limited. https://books.google.com.sg/books?id=HM5jPQAACAAJ

[32] Alexander Heinrich, Milan Stute, and Matthias Hollick. 2021. OpenHaystack: a framework for tracking personal bluetooth devices via Apple's massive find my network. In *Proceedings of the 14th ACM Conference on Security and Privacy in Wireless and Mobile Networks* (Abu Dhabi, United Arab Emirates) *(WiSec '21)*. Association for Computing Machinery, New York, NY, USA, 374–376. https://doi.org/10.1145/3448300.3468251

[33] Signal Hound. 2023. BB60C Signal Analyzer. https://signalhound.com/sigdownloads/datasheets/Signal-Hound-BB60C-Data-Sheet.pdf. [Accessed: 2025-04-20].

[34] Jia Hu, Linling Zhong, Tao Ma, Zhe Ding, and Zhanqi Xu. 2022. Long-Range FM Backscatter Tag With Tunnel Diode. *IEEE Microwave and Wireless Components Letters* 32, 1 (2022), 92–95. https://doi.org/10.1109/LMWC.2021.3117033

[35] Info-communications Media Development Authority. 2016. Technical Specification for White Space Devices. https://www.imda.gov.sg/-/media/imda/files/regulation-licensing-and-consultations/ict-standards/telecommunication-standards/radio-comms/imda-ts-wsd.pdf [Accessed: 2024-10-29].

[36] Texas Instrumenets. 2025. MSP430FR5959 Microcontroller. https://www.ti.com/lit/ds/symlink/msp430fr5959.pdf. [Accessed: 2025-04-20].

[37] Vikram Iyer, Vamsi Talla, Bryce Kellogg, Shyamnath Gollakota, and Joshua Smith. 2016. Inter-Technology Backscatter: Towards Internet Connectivity for Implanted Devices. In *Proceedings of the 2016 ACM SIGCOMM Conference* (Florianopolis, Brazil) *(SIGCOMM '16)*. Association for Computing Machinery, New York, NY, USA, 356–369. https://doi.org/10.1145/2934872.2934894

[38] Bryce Kellogg, Aaron Parks, Shyamnath Gollakota, Joshua R. Smith, and David Wetherall. 2014. Wi-Fi Backscatter: Internet Connectivity for RF-Powered Devices. In *Proceedings of the 2014 ACM Conference on SIGCOMM* (Chicago, Illinois, USA) *(SIGCOMM '14)*. Associationfor Computing Machinery, New York, NY, USA, 607–618. https://doi.org/10.1145/2619239.2626319

[39] Bryce Kellogg, Vamsi Talla, and Shyamnath Gollakota. 2014. Bringing gesture recognition to all devices. In *Proceedings of the 11th USENIX Conference on Networked Systems Design and Implementation* (Seattle, WA) *(NSDI'14)*. USENIX Association, USA, 303–316. https://www.usenix.org/conference/nsdi14/technical-sessions/presentation/kellogg

[40] Bryce Kellogg, Vamsi Talla, Shyamnath Gollakota, and Joshua R. Smith. 2016. Passive Wi-Fi: Bringing Low Power to Wi-Fi Transmissions. In *Proceedings of the 13th Usenix Conference on Networked Systems Design and Implementation* (Santa Clara, CA) *(NSDI'16)*. USENIX Association. https://www.usenix.org/conference/nsdi16/technical-sessions/presentation/kellogg

[41] W. Ko, W. Thompson, and E. Yon. 1963. Tunnel diode FM transmitter for medical research and laboratory telemetering. *Med. Electron. Biol. Engng* (1963), 363–369. https://doi.org/10.1007/BF02474419

[42] Tianxing Li, Chuankai An, Zhao Tian, Andrew T. Campbell, and Xia Zhou. 2015. Human Sensing Using Visible Light Communication. In *Proceedings of the 21st Annual International Conference on Mobile Computing and Networking* (Paris, France) *(MobiCom '15)*. Association for Computing Machinery, New York, NY, USA, 331–344. https://doi.org/10.1145/2789168.2790110

[43] Tianxing Li, Xi Xiong, Yifei Xie, George Hito, Xing-Dong Yang, and Xia Zhou. 2017. Reconstructing Hand Poses Using Visible Light. *Proc. ACM Interact. Mob. Wearable Ubiquitous Technol.* 1, 3, Article 71 (Sept. 2017), 20 pages. https://doi.org/10.1145/3130937

[44] Jaime Lien, Nicholas Gillian, M. Emre Karagozler, Patrick Amihood, Carsten Schwesig, Erik Olson, Hakim Raja, and Ivan Poupyrev. 2016. Soli: ubiquitous gesture sensing with millimeter wave radar. *ACM Trans. Graph.* 35, 4, Article 142 (July 2016), 19 pages. https://doi.org/10.1145/2897824.2925953

[45] Vincent Liu, Aaron Parks, Vamsi Talla, Shyamnath Gollakota, David Wetherall, and Joshua R. Smith. 2013. Ambient Backscatter: Wireless Communication out of Thin Air. In *Proceedings of the ACM SIGCOMM 2013 Conference on SIGCOMM* (Hong Kong, China) *(SIGCOMM '13)*. Association for Computing Machinery, New York, NY, USA, 39–50. https://doi.org/10.1145/2486001.2486015

[46] Ludlows. 2021. PESQ: Perceptual Evaluation of Speech Quality. https://github.com/ludlows/PESQ/tree/v0.0.4. [Accessed: 2025-01-29].

[47] Sooriya Patabandige Pramuka Medaranga, Rajashekar Reddy Chinthalapani, Wenqing Yan, Prabal Dutta, and Ambuj Varshney. 2025. Unraveling the Missing Link in Low-power Communication: An Autodyning Receiver Architecture that Achieves a Long Range. In *Proceedings of the 23rd Annual International Conference on Mobile Systems, Applications and Services* (Anaheim, CA, USA) *(MobiSys '25)*. Association for Computing Machinery, New York, NY, USA, To Appear. https://doi.org/10.1145/3711875.3729164

[48] Mediacorp. [n. d.]. List of radio stations in Singapore. https://cnalifestyle.channelnewsasia.com/entertainment/mediacorp-radio-station-nielsen-rating-survey-2023-yes-933-345911. [Accessed: 2024-07-02].

[49] Muhammad Sarmad Mir, Wenqing Yan, Prabal Dutta, Domenico Giustiniano, and Ambuj Varshney. 2023. TunnelLiFi: Bringing LiFi to Commodity Internet of Things Devices. In *Proceedings of the 24th International Workshop on Mobile Computing Systems and Applications* (Newport Beach, California) *(HotMobile '23)*. Association for Computing Machinery, New York, NY, USA, 1–7. https://doi.org/10.1145/3572864.3580327

[50] G. T. Munsterman. 1965. Tunnel-Diode Microwave Amplifiers. *APL Technical Digest* (1965).

[51] Saman Naderiparizi, Mehrdad Hessar, Vamsi Talla, Shyamnath Gollakota, and Joshua R Smith. 2018. Towards Battery-Free HD Video Streaming. In *15th USENIX Symposium on Networked Systems Design and Implementation (NSDI 18)*. USENIX Association, Renton, WA.

[52] Saman Naderiparizi, Aaron N. Parks, Zerina Kapetanovic, Benjamin Ransford, and Joshua R. Smith. 2015. WISPCam: A battery-free RFID camera. In *2015 IEEE International Conference on RFID (RFID)*. 166–173. https://doi.org/10.1109/RFID.2015.7113088

[53] Sujay Narayana, R. Venkatesha Prasad, Vijay S. Rao, T. V. Prabhakar, Sripad S. Kowshik, and Madhuri Sheethala Iyer. 2015. PIR sensors: characterization and novel localization technique. In *Proceedings of the 14th International Conference on Information Processing in Sensor Networks* (Seattle, Washington) *(IPSN '15)*. Association for Computing Machinery, New York, NY, USA, 142–153. https://doi.org/10.1145/2737095.2742561

[54] Unkyu Park and John Heidemann. 2011. Data muling with mobile phones for sensornets. In *Proceedings of the 9th ACM Conference on Embedded Networked Sensor Systems* (Seattle, Washington) *(SenSys '11)*. Association for Computing Machinery, New York, NY, USA, 162–175. https://doi.org/10.1145/2070942.2070960

[55] Yao Peng, Longfei Shangguan, Yue Hu, Yujie Qian, Xianshang Lin, Xiaojiang Chen, Dingyi Fang, and Kyle Jamieson. 2018. PLoRa: a passive long-range data network from ambient LoRa transmissions. In *Proceedings of the 2018 Conference of the ACM Special Interest Group on Data Communication* (Budapest, Hungary) *(SIGCOMM '18)*. Association for Computing Machinery, New York, NY, USA, 147–160. https://doi.org/10.1145/3230543.3230567

[56] Carlos Pérez-Penichet, Frederik Hermans, Ambuj Varshney, and Thiemo Voigt. 2016. Augmenting IoT Networks with Backscatter-Enabled Passive Sensor Tags. In *Proceedings of the 3rd Workshop on Hot Topics in Wireless* (New York City, New York) *(HotWireless '16)*. Association for Computing Machinery, New York, NY, USA, 23–27. https://doi.org/10.1145/2980115.2980132

[57] Alec Radford, Jong Wook Kim, Tao Xu, Greg Brockman, Christine McLeavey, and Ilya Sutskever. 2022. Robust Speech Recognition via Large-Scale Weak Supervision. arXiv:2212.04356 [eess.AS] https://arxiv.org/abs/2212.04356

[58] World Radio. [n. d.]. List of radio stations in the San Francisco. https://worldradiomap.com/us-ca/san-francisco. [Accessed: 2024-07-02].

[59] Radiostationworld. [n. d.]. Canada: Ontario: Radio Station Market List. http://radiostationworld.com/Locations/Canada/Ontario/default.asp. [Accessed: 2024-07-02].

[60] Sreeraj Rajendran, Roberto Calvo-Palomino, Markus Fuchs, Bertold Van den Bergh, Hector Cordobes, Domenico Giustiniano, Sofie Pollin, and Vincent Lenders. 2018. Electrosense: Open and Big Spectrum Data. *IEEE Communications Magazine* 56, 1 (2018), 210–217. https://doi.org/10.1109/MCOM.2017.1700200

[61] Yordan P. Raykov, Emre Ozer, Ganesh Dasika, Alexis Boukouvalas, and Max A. Little. 2016. Predicting room occupancy with a single passive infrared (PIR) sensor through behavior extraction. In *Proceedings of the 2016 ACM International Joint Conference on Pervasive and Ubiquitous Computing* (Heidelberg, Germany) *(UbiComp '16)*. Association for Computing Machinery, New York, NY, USA, 1016–1027. https://doi.org/10.1145/2971648.2971746

[62] Kyle Rector, Keith Salmon, Dan Thornton, Neel Joshi, and Meredith Ringel Morris. 2017. Eyes-Free Art: Exploring Proxemic Audio Interfaces For Blind and Low Vision Art Engagement. *Proc. ACM Interact. Mob. Wearable Ubiquitous Technol.* 1, 3, Article 93 (Sept. 2017), 21 pages. https://doi.org/10.1145/3130958

[63] Chandan K A Reddy, Vishak Gopal, and Ross Cutler. 2022. Dnsmos P.835: A Non-Intrusive Perceptual Objective Speech Quality Metric to Evaluate Noise Suppressors. In *ICASSP 2022 - 2022 IEEE International Conference on Acoustics, Speech and Signal Processing (ICASSP)*. 886–890. https://doi.org/10.1109/ICASSP43922.2022.9746108

[64] C. Rajashekar Reddy, Manoj Gulati, and Ambuj Varshney. 2023. Beyond Broadcasting: Revisiting FM Frequency-band for Providing Connectivity to Next Billion Devices. In *Proceedings of the 11th International Workshop on Energy Harvesting & Energy-Neutral Sensing Systems* (Istanbul, Turkiye) *(ENSsys '23)*. Association for Computing Machinery, New York, NY, USA, 30–36. https://doi.org/10.1145/3628353.3628546

[65] A. W. Rix, J. G. Beerends, M. P. Hollier, and A. P. Hekstra. 2001. Perceptual evaluation of speech quality (PESQ)-a new method for speech quality assessment of telephone networks and codecs. In *2001 IEEE International Conference on Acoustics, Speech, and Signal Processing. Proceedings (Cat. No.01CH37221)*, Vol. 2. 749–752 vol.2. https://doi.org/10.1109/ICASSP.2001.941023

[66] RTL-SDR.com. 2024. RTL-SDR Blog V4 Datasheet. https://www.rtl-sdr.com/wp-content/uploads/2024/12/RTLSDR_V4_Datasheet_V_1_0.pdf [Accessed: 2025-02-01].

[67] Abusayeed Saifullah, Mahbubur Rahman, Dali Ismail, Chenyang Lu, Ranveer Chandra, and Jie Liu. 2016. SNOW: Sensor Network over White Spaces. In *Proceedings of the 14th ACM Conference on Embedded Network Sensor Systems CD-ROM* (Stanford, CA, USA) *(SenSys '16)*. Association for Computing Machinery, New York, NY, USA, 272–285. https://doi.org/10.1145/2994551.2994552

[68] Nordic Semiconductor. 2025. nRF52840 Product Specification v1.11. https://docs.nordicsemi.com/bundle/ps_nrf52840/page/keyfeatures_html5.html. [Accessed: 2025-01-22].

[69] Nordic Semiconductor. 2025. Power Profiler Kit II. https://docs.nordicsemi.com/bundle/ug_ppk2/page/UG/ppk/PPK_user_guide_Intro.html. [Accessed: 2025-04-20].

[70] RCA Corporation. Semiconductor and Materials Division. 1963. *RCA Tunnel Diode Manual*. RCA.

[71] Semtech. 2025. Semtech SX1276 LoRa Core 137MHz to 1020MHz Long Range Low Power Transceiver. https://semtech.my.salesforce.com/sfc/p/#E0000000JelG/a/2R0000001Rbr/6EfVZUorrpoKFfvaF_Fkpgp5kzjiNyiAbqcpqh9qSjE. [Accessed: 2025-01-22].

[72] Skyworks Solutions. 2023. Si4712/13-B30 Data Sheet. https://www.skyworksinc.com/-/media/Skyworks/SL/documents/public/data-sheets/Si4712-13-B30.pdf. [Accessed: 2023-10-01].

[73] SpeechMOS. 2023. SpeechMOS: A Python Package for PESQ and MOS. https://pypi.org/project/speechmos/#description. [Accessed: 2025-01-30].

[74] Swissinfo.ch. [n. d.]. Swiss Broadcasting Corporation pulls plug on FM radio. https://www.swissinfo.ch/eng/life-aging/swiss-broadcasting-corporation-pulls-plug-on-fm-radio/88663569. [Accessed: 2025-01-31].

[75] Vamsi Talla, Mehrdad Hessar, Bryce Kellogg, Ali Najafi, Joshua R. Smith, and Shyamnath Gollakota. 2017. LoRa Backscatter: Enabling The Vision of Ubiquitous Connectivity. *Proc. ACM Interact. Mob. Wearable Ubiquitous Technol.* 1, 3, Article 105 (Sept. 2017), 24 pages. https://doi.org/10.1145/3130970

[76] Vamsi Talla, Bryce Kellogg, Shyamnath Gollakota, and Joshua R. Smith. 2017. Battery-Free Cellphone. *Proc. ACM Interact. Mob. Wearable Ubiquitous Technol.* 1, 2, Article 25 (June 2017), 20 pages. https://doi.org/10.1145/3090090

[77] Vamsi Talla and Joshua R Smith. 2013. Hybrid analog-digital backscatter: A new approach for battery-free sensing. In *2013 IEEE international conference on RFID (RFID)*. IEEE, 74–81. https://doi.org/10.1109/RFID.2013.6548138

[78] Lim Chang Quan Thaddeus, C. Rajashekar Reddy, Yuvraj Singh Bhadauria, Dhairya Shah, Manoj Gulati, and Ambuj Varshney. 2024. TunnelSense: Low-Power, Non-Contact Sensing Using Tunnel Diodes. In *2024 IEEE International Conference on RFID (RFID)*. 154–159. https://doi.org/10.1109/RFID62091.2024.10582671

[79] Tijs van Dam and Koen Langendoen. 2003. An adaptive energy-efficient MAC protocol for wireless sensor networks. In *Proceedings of the 1st International Conference on Embedded Networked Sensor Systems* (Los Angeles, California, USA) *(SenSys '03)*. Association for Computing Machinery, New York, NY, USA, 171–180. https://doi.org/10.1145/958491.958512

[80] Ambuj Varshney and Lorenzo Corneo. 2020. Tunnel Emitter: Tunnel Diode Based Low-Power Carrier Emitters for Backscatter Tags. In *Proceedings of the 26th Annual International Conference on Mobile Computing and Networking* (London, United Kingdom) *(MobiCom '20)*. Association for Computing Machinery, New York, NY, USA, Article 42, 14 pages. https://doi.org/10.1145/3372224.3419199

[81] Ambuj Varshney, Oliver Harms, Carlos Pérez-Penichet, Christian Rohner, Frederik Hermans, and Thiemo Voigt. 2017. LoRea: A Backscatter Architecture That Achieves a Long Communication Range. In *Proceedings of the 15th ACM Conference on Embedded Network Sensor Systems* (Delft, Netherlands) *(SenSys '17)*. Association for Computing Machinery, New York, NY, USA, Article 18, 14 pages. https://doi.org/10.1145/3131672.3131691

[82] Ambuj Varshney, Andreas Soleiman, Luca Mottola, and Thiemo Voigt. 2017. Battery-free Visible Light Sensing. In *Proceedings of the 4th ACM Workshop on Visible Light Communication Systems* (Snowbird, Utah, USA) *(VLCS '17)*. Association for Computing Machinery, New York, NY, USA, 3–8. https://doi.org/10.1145/3129881.3129890

[83] Ambuj Varshney, Andreas Soleiman, and Thiemo Voigt. 2019. TunnelScatter: Low Power Communication for Sensor Tags Using Tunnel Diodes. In *The 25th Annual International Conference on Mobile Computing and Networking* (Los Cabos, Mexico) *(MobiCom '19)*. Association for Computing Machinery, New York, NY, USA, Article 50, 17 pages. https://doi.org/10.1145/3300061.3345451

[84] Ambuj Varshney, Wenqing Yan, and Prabal Dutta. 2022. Judo: Addressing the Energy Asymmetry of Wireless Embedded Systems through Tunnel Diode Based Wireless Transmitters. In *Proceedings of the 20th Annual International Conference on Mobile Systems, Applications and Services* (Portland, Oregon) *(MobiSys '22)*. Association for Computing Machinery, New York, NY, USA, 273–286. https://doi.org/10.1145/3498361.3538923

[85] Deepak Vasisht, Zerina Kapetanovic, Jong-ho Won, Xinxin Jin, Ranveer Chandra, Ashish Kapoor, Sudipta N. Sinha, Madhusudhan Sudarshan, and Sean Stratman. 2017. Farmbeats: an IoT platform for data-driven agriculture. In *Proceedings of the 14th USENIX Conference on Networked Systems Design and Implementation* (Boston, MA, USA) *(NSDI'17)*. USENIX Association, USA, 515–528. https://www.usenix.org/conference/nsdi17/technical-sessions/presentation/vasisht

[86] Raghav H. Venkatnarayan and Muhammad Shahzad. 2018. Gesture Recognition Using Ambient Light. *Proc. ACM Interact. Mob. Wearable Ubiquitous Technol.* 2, 1, Article 40 (March 2018), 28 pages. https://doi.org/10.1145/3191772

[87] Anandghan Waghmare, Qiuyue Xue, Dingtian Zhang, Yuhui Zhao, Shivan Mittal, Nivedita Arora, Ceara Byrne, Thad Starner, and Gregory D Abowd. 2020. UbiquiTouch: Self Sustaining Ubiquitous Touch Interfaces. *Proc. ACM Interact. Mob. Wearable Ubiquitous Technol.* 4, 1, Article 27 (mar 2020), 22 pages. https://doi.org/10.1145/3380989

[88] Anran Wang, Vikram Iyer, Vamsi Talla, Joshua R. Smith, and Shyamnath Gollakota. 2017. FM Backscatter: Enabling Connected Cities and Smart Fabrics. In *Proceedings of the 14th USENIX Conference on Networked Systems Design and Implementation* (Boston, MA, USA) *(NSDI'17)*. USENIX Association, USA, 243–258. https://www.usenix.org/conference/nsdi17/technical-sessions/presentation/wang-anran

[89] Ju Wang, Omid Abari, and Srinivasan Keshav. 2018. Challenge: RFID Hacking for Fun and Profit. In *Proceedings of the 24th Annual International Conference on Mobile Computing and Networking* (New Delhi, India) *(MobiCom '18)*. Association for Computing Machinery, New York, NY, USA, 461–470. https://doi.org/10.1145/3241539.3241561

[90] Lei Wang, Meng Chen, Li Lu, Zhongjie Ba, Feng Lin, and Kui Ren. 2023. VoiceListener: A Training-free and Universal Eavesdropping Attack on Built-in Speakers of Mobile Devices. *Proc. ACM Interact. Mob. Wearable Ubiquitous Technol.* 7, 1, Article 32 (March 2023), 22 pages. https://doi.org/10.1145/3580789

[91] Roy Want. 2006. An introduction to RFID technology. *IEEE Pervasive Computing* 5, 1 (2006), 25–33. https://doi.org/10.1109/MPRV.2006.2

[92] Radio World. [n. d.]. Switching off FM in Norway, and soon Switzerland. https://www.radioworld.com/news-and-business/switching-off-fm-in-norway-and-soon-switzerland. [Accessed: 2025-01-31].

[93] Pengyu Zhang, Dinesh Bharadia, Kiran Joshi, and Sachin Katti. 2016. HitchHike: Practical Backscatter Using Commodity WiFi. In *Proceedings of the 14th ACM Conference on Embedded Network Sensor Systems* (Stanford, CA, USA) *(SenSys '16)*. Association for Computing Machinery, New York, NY, USA, 259–271. https://doi.org/10.1145/2994551.2994565

[94] Pengyu Zhang, Pan Hu, Vijay Pasikanti, and Deepak Ganesan. 2015. EkhoNet: High-Speed Ultra Low-Power Backscatter for Next Generation Sensors. *GetMobile: Mobile Comp. and Comm.* 19, 2 (Aug. 2015), 14–17. https://doi.org/10.1145/2817761.2817766

[95] Pengyu Zhang, Mohammad Rostami, Pan Hu, and Deepak Ganesan. 2016. Enabling Practical Backscatter Communication for On-body Sensors. In *Proceedings of the 2016 ACM SIGCOMM Conference* (Florianopolis, Brazil) *(SIGCOMM '16)*. Association for Computing Machinery, New York, NY, USA, 370–383. https://doi.org/10.1145/2934872.2934901

[96] Jia Zhao, Wei Gong, and Jiangchuan Liu. 2021. Microphone array backscatter: an application-driven design for lightweight spatial sound recording over the air. In *Proceedings of the 27th Annual International Conference on Mobile Computing and Networking* (New Orleans, Louisiana) *(MobiCom '21)*. Association for Computing Machinery, New York, NY, USA, 710–722. https://doi.org/10.1145/3447993.3483265